Università degli Studi della Calabria

Dottorato di Ricerca in Ingegneria
dei Sistemi ed Informatica
XXII Ciclo

Innovative control architectures of power interfacing systems for distributed generation applications

Domenico Sgró

A.A. 2008-2009

Il tutor
Prof. Ciro Picardi

Il coordinatore
Prof. Luigi Palopoli

DIPARTIMENTO DI ELETTRONICA
INFORMATICA E SISTEMISTICA
Settore Scientifico Disciplinare: ING-IND/32

Domenico Sgró

Innovative control architectures of power interfacing systems for distributed generation applications

Ph.D. Thesis

Springer
Berlin Heidelberg New York
Hong Kong London
Milan Paris Tokyo

Author's Address:
Domenico Sgró
Dip. di Elettronica, Informatica e Sistemistica,Cubo 42C
Università degli Studi della Calabria
Via Pietro Bucci
I-87036 Rende, Italy, EU
e-mail: dsgro@deis.unical.it

Contents

References 101

Introduction

Recently, the number of equipments based on power electronic converters connected to the grid like Uninterrupted Power Supply (UPS) or Inverter, used as power interface between power sources and the grid, is constantly increasing. The main causes of this phenomenon are the ever increasing energy demand and the pollution due to the use of fossil fuels, as well as the problems connected to the future availability of coal, oil and gas.

In fact, global energy consumption in the last half century has increased very rapidly and is expected to continue to grow over the next 50 years. However, it is a widespread opinion we will see significant differences between the last 50 years and the next. Relatively cheap fossil fuels and increased rates of industrialization in North America, Europe, and Japan encouraged the rise of energy demand in the last five decades; yet while energy consumption in these countries continues to increase, additional factors are making the picture for the next 50 years more complex. These additional complicating factors include the very rapid increase in energy use in China and India (countries representing about a third of the worlds population), the expected depletion of oil resources in the not-too-distant future, and the effect of human activities on global climate change [14].

As the International Energy Agency (IEA) reports in the World Energy Outlook 2004, the total primary energy demand in the world increased from 5536 GTOE[1] (GigaTons of Oil Equivalent) in 1971 to 10345 GTOE in 2002, that mens an average annual increase of 2% (see Tab. 0.1).

Energy consumption data from British Petroleum Corp. (BP), confirmed the average increase of 2% in the decade from 1996 to 2006. However, more significant data[2] are shown in Tab. 0.2. These data show that the growth of world total energy consumption from 2000 to 2005 was 2.8% per year. Moreover, others sources report the increases from 2003 to 2004 being 4.3% [42],[17], evidencing as the increment of the rate of growth is mainly due to the rapid increase in the developing countries and in particular in Pa-

Table 0.1. World Total Energy Demand by source type

Energy Source Type	1971 (MTOE)	2002 (MTOE)	Annual Percentage of Change 1971 ÷ 2002
Coal	1407	2389	+1.7
Oil	2413	3676	+1.4
Gas	892	2190	+2.9
Nuclear	29	892	+11.6
Hydro	104	224	+2.5
Biomass and Waste	687	1119	+1.6
Other Renewables	4	55	+8.8
Total	5536	10345	+2.0

[1] 1 GTOE = 10^9 TOE (Tons of Oil Equivalent). 1 TOE = 42 GJ. Others multiples of TOE are MTOE, 1 MTOE = 10^6 TOE, and KTOE, 1 KTOE = 10^3 TOE.

[2] Source:International Energy Agency (IEA) Statistics Division, 2006. Energy Balances of OECD Countries (2006 edition) and Energy Balances of Non-OECD Countries (2006 edition). Paris: IEA.

Table 0.2. World Energy Demand by region

Region/Classification	2005 (KTOE)	2000 (KTOE)	Annual Percentage of Change 2000 ÷ 2005
Asia (excluding Middle East)	3892874	3025401	+5.7
Central America and Caribbean	241128	209534	+3.0
Europe	2738321	2582180	+1.2
Middle East and North Africa	728733	575914	+5.3
Central America and Caribbean	728733	575914	+5.3
North America	2615539	2554649	+0.5
South America	428765	390444	+2.0
Developed Countries	6335685	6072283	+0.9
Developing Countries	4875673	3761588	+5.9
World	11433918	10029174	+2.8

cific Asia. Among these countries, China and India increased their primary energy consumption from 2003 to 2004 by 14% and 8% respectively. More recently, in the the period from 2005 to 2007 China, India and all the Pacific Asia pulled worldwide energy consumption confirming the estimation of a worldwide average annual growth among $1.6\% \div 2.5\%$ [40],[41].

In the last year, in spite of the recent economic crisis, primary energy consumption kept growing, as did growth for each of the fossil fuels. All the net growth in energy consumption came from the rapidly industrializing non-OECD (Organization for Economic Co-operation and Development) economies, with China alone accounting for nearly three-quarters of global growth. For the first time, non-OECD energy consumption surpassed OECD consumption. For a sixth consecutive year, coal was the fastest-growing fuel with obvious implications for global CO_2 emissions.

Based on a 2% increase per year (average of the estimates from other sources), the primary energy demand of 10345 GTOE in 2002 would double by 2037 and triple by 2057. With such high energy demand expected 50 years from now, it is important to

look at all of the available strategies to fulfill the future demand, especially for electricity and transportation.

Some other important consideration are related to the future availability of fossil energy sources. Fossil fuels such as natural gas, petroleum, hard and brown coal needed many thousands of years to form. Organic substances (i.e. animal or vegetable residues) were the base materials. Hence, fossil fuels are stored biomass of the ancient past. A huge amount of these fossil fuels has already been consumed in the 20th century. However, due to the increasing exploitation of the fossil reservoirs, future extraction will be more and more difficult, technically challenging and risky and therefore much more expensive than today. Deep-sea oil rigs are one step in this development. If fossil fuel use continues unchecked, all available reserves of oil and natural gas could be exploited within the 21st century. Only coal reserves will be available for a longer period of time. Thus, some decades from now, a few generations of humanity will have exploited the whole fossil energy reserves that required millions of years to form. Future generations will no longer have the opportunity to use fossil fuels as their energy supply.

An exact estimation of the existing reserves of fossil energy resources is very difficult, because only the size of deposits already explored is known. Additional reserves to be discovered in future can only be estimated. However, even if major fossil fuel reserves should be discovered, this would not change the fact that fossil fuel reserves are limited. The time span of their availability can be extended only by some years or decades at best [49].

However, even though there are widely differing views and estimates of the ultimately recoverable resources of fossil fuels, it is fair to say that they may last for around $50 \div 150$ years with a peak in production occurring much earlier. Nonetheless a big concern is the climatic threat of additional carbon that will be released into the atmosphere. According to the estimates from the IEA, if the present shares of fossil fuels are maintained up to 2030 without any carbon sequestration, a cumulative amount of approximately

1000 gigatons of carbon will be released into the atmosphere. This is especially troublesome in view of the fact that the present total cumulative emissions of about 300 gigatons of carbon have already raised serious concerns about global climate change [14].

As consequent of the illustrated scenario, there is registered a massive interest on all those energy sources defined "alternative" or "non-conventional". In particular, the attention of the scientific community and of some industrial sectors is been focused on the renewable energy sources, i.e. all those sources available in unlimited quantity, e.g. photovoltaic and wind, or that can be replenished in times compatible with those in which human activities are carried out, like biogas,biomass or mini-hydro. Many studies show that the global wind resource technically recoverable is more than twice as much as the projection for the worlds electricity demand in 2020. Similarly, theoretical solar energy potential corresponds to almost $90,000,000$ MTOE per year, which is almost $10,000$ times the world total primary energy supply [6],[11].

However, in spite of the huge availability of these sources, in the past years their development has been restrained by several problems, some of them connected with the problem of storage the energy supplied and/or with the difficulty to convert the energy produced by these sources in energy for the Electrical Power Systems(EPS). In particular, both low efficiency and high cost of conversion obstructed for years the possibility of diffusion of many renewable energy sources, so that, it is a common accepted idea, the development of more effective interface systems based on power electronic converters, triggered the recent diffusion of relatively small generation systems powered by renewables.

The main differences between power electronics based interfaces and conventional synchronous generators lie in the ability of power converters to face critical conditions and sudden changes in the grid currents and voltages. Moreover, power electronics converter, like suitable grid-connected inverter, can be connected both in three phases and single phase systems. These abilities

make generation systems based on power converter particularly adapt to applications at the distribution level, triggering important changes that, in the opinion of many, would bring to the decentralization of the generation units.

The role played by power electronic interfaces, in the diffusion of Distributed Generation (DG) systems powered by renewables, becomes more clear considering that many renewable sources are more suitable for distributed applications. As example, in the case of photovoltaic power sources the same amount of energy could be obtained with a big power plant or with many small power plants; in the first case a big surface dedicated to the installation of the photovoltaic generator is necessary as well as a transmission system in order to transfer the energy produced to the loads; in the second case many small power generators could be installed near the loads using marginal surfaces like building facade and roof. Many studies demonstrate as the second solution has several advantages in terms of effectiveness, efficiency and peach shaving. Moreover, wind and mini-hydro power plants have to be located in specific areas where the primary resource of power (wind power or water power) is available. As Further examples, it is important to underline that in terms of sustainable development, many small biomass power plants, which utilize resource of a relatively small area, should be preferred with respect to a large one which gathers resource in a vast area.

As a consequence of the aforementioned considerations, the conversion from a centralized generation system to a distribution system based on DG sources is inevitable, if energy supplied by renewables have to become a relevant share of the total world energy production. However, also considering the present contribution of power electronic interfaces to the development and deployment of renewable technologies, there are challenges, regarding the integration of renewable sources into the EPSs, still far to be solved.

Objectives of the work

Today, the planning and development of integrated energy must consider not only the environment itself and the existence of energy sources where it is desirable to install a renewable energy source, but also local needs and set-up of the distribution system. In particular, characteristics and number of loads and generators near the hypothetical point of installation are basic information. The knowledge of local needs and set-up is necessary because the presence in a certain area of many DG sources which produce an important share of the local required energy, can involve instability and security problems on the grid. This is mainly due to the difficulty to predict and schedule the powers generated by DGs.

In fact, in the modern EPSs small DG sources are still considered merely as "active loads". This means that many services as voltage control or reactive supply do not make use of the contribution of small generator sources which should operate virtually without influence grid parameters, like voltage amplitude and frequency. However, it is beyond doubt that the presence of many small generators involve important influences on the aforementioned parameters. Then, it should be preferable that all the DG sources of a distribution system give a contribute to maintain grid parameters near the correct values.

The possibility to perform service as voltage and reactive control at distribution level is a peculiar ability of power electronic converter, then for these reasons there is an increasing interest in power control strategies for suitable Grid-connected inverter operating as power interface between the grid and the power source.

Centered in the field of the renewable energy sources, this work deal with the analysis of innovative control architectures of power interfacing systems based on static converters for distributed generation applications. The main aim is to present and discuss the analysis techniques and the strategy controls, for grid-connected inverter, carried out during the Ph.D course.

Renewable energy generation systems, based on photovoltaic sources, wind turbines or fuel-cells, nowadays represent the most

promising solution to reduce the consumption of oil and gas. These sources require a suitable power conversion system to manage the generated energy. Actually, the grid-connected configuration of this power conversion system is economically very attractive, because many European countries are providing money incentives for the energy produced by renewable sources and delivered to the utility grid. However, their development and full integration make rise problems, some of which will be dealt with in the following chapters.

Plan of the work

The thesis is organized as it follows.

- Chapter 1 deals with some of the main synchronization methods applied in the considered research field and presents a power electrical signal tracking strategy consisting in the combined use of a simple and robust frequency estimation method based on modulating functions and an orthogonal system generator including the second-order generalized integrator. The proposed strategy has the advantages of a fast and accurate signal tracking capability and a good rejection to noise due to the low-pass filter properties of the modulating functions. The effectiveness of the proposed method is validated through comparisons with existing methods performing simulated and laboratory experiments.
- In Chapter 2 This chapter presents a new approach to model the electrical signals in power systems. The approach is based on the concept, derived from differential geometry, of contact between a signal and an osculating sinusoid. A direct application leads to a synchronization algorithm performing tasks comparable to those of single-phase PLL as verified by some different simulation results. Moreover, a significant advantage of the approach is the possibility to define quantities typically

considered in sinusoidal steady state conditions also during the transients.

- In Chapter 3 deals with a new control strategy for a pulse width modulation (PWM) three-phase voltage source inverter (VSI) connected to the grid and able to support bi-directional power flow. In particular, the proposed strategy is developed so as to combine the advantages of the Current Control and the Voltage Control. The effectiveness of this combined control strategy is proved by some numerical results compared with those obtained applying only the conventional current control strategy.
  Moreover a Microgrid application of the control strategy in presented.

1

Synchronization methods

For correct operation in grid-connected condition, distributed generation systems need the information about amplitude, phase angle, and frequency of the grid fundamental voltages and currents. Since noise, harmonic pollution, and frequency variations are common problems in the utility grid, then it is necessary to have systems able to extract information about the fundamental values from highly distorted signals. For these reasons, robust and accurate estimation and synchronization methods are necessary to obtain the aforementioned information also in noise environmental. This chapter deal with some of the main synchronization methods applied in the considered research field and presents a power electrical signal tracking strategy consisting in the combined use of a simple and robust frequency estimation method based on modulating functions and an orthogonal system generator including the second-order generalized integrator. The proposed strategy has the advantages of a fast and accurate signal tracking capability and a good rejection to noise due to the low-pass filter properties of the modulating functions. The effectiveness of the proposed method is validated through comparisons with existing methods performing simulated and laboratory experiments.

1.1 Introduction

Detection of frequency, phase angle, and amplitude of currents and voltages, in the electric power systems, is one of the most important issues regarding the development of power conditioning equipment such as UPS, series or shunt compensators, and distributed generation systems based on grid connected inverters [29],[54],[53],[25],[45]. In particular, in this last application, an accurate and fast detection of the phase angle of the utility voltage is essential to assure the synchronization between the power generation systems and the distribution grid. Moreover, it is important to observe that line notching, voltage unbalance, line dips, phase loss, harmonic pollutions, and frequency variations are common conditions faced by the equipment interfacing with electric utility. Therefore, information about frequency, amplitude, and phase angle of grid voltages and currents are necessary to assure the correct generation of the reference signals and to avoid security problems on the grid (Anti-islanding protection) [10],[9],[37],[35]. The same information can be used to synchronize the turning on/off of the power devices and to calculate and control the flow of active and reactive powers [1] or to allow a continuous monitoring of the grid state [33].

For these reasons, there is an increasing interest in synchronization algorithms in order to monitor and control the dynamics of the electric power systems. Among the first techniques for frequency measurement, there were those based on zero crossing [50],[12],[56]. They were gradually abandoned due to their sensitivity to noise, presence of dc components in the signal, and harmonics [38]. The most commonly employed approach is based on phase-locked-loop (PLL) topologies for grid-connected systems [7],[30],[18],[21],[36], [24],[23],[30],[34],[32] which are standard defacto in power systems.

The structure of the main PLL topology is a feedback control system that automatically adjusts the phase of a locally generated signal to match the phase of an input signal. In this topology, the generation of an orthogonal voltage system is required. In the

three-phase systems, orthogonal reference signals can be obtained by the Clarke transformation applied on the values of the phase voltages [29],[25],[30]. Instead, in single-phase systems, there is less information than in three-phase systems regarding the grid condition, so advanced methods to create an orthogonal voltage system have been presented in literature [33],[34],[32].

An interesting and effective method to create an orthogonal voltage system is presented in [34], where a second-order generalized integrator (SOGI) is used. By means of SOGI, the input signal is also filtered resulting two clean orthogonal voltages waveforms. For its correct operation, SOGI needs the information about the grid frequency that can be obtained through the feedback closed loop of the PLL; this involves that the global system behavior will be affected by SOGI and PLL transients. It is worth to note that even if PLL-based methods seem the easiest to use in real-time operation, they exhibit a longer transient time than some fast digital algorithms such as, for example, those based on Fast Fourier Transform. This constitutes a limitation for those applications which require very fast transient period [36]. Moreover, PLL requires an initial condition, relative to the starting frequency, which has to be very close to the real one, in order to lock the signal in a fast way.

However, zero-crossing and PLL methods are not the only methods to deal with synchronization problems. In [3], a recursive discrete Fourier transform (RDFT) filter is used for power converter grid synchronization with two compensation approaches in case of discrepancy between the time window of the filter and the system period of the grid. A detailed comparison of the PLL-based methods with RDFT and discrete Kalman filtering (DKF) in terms of computational burden, reliability in the detection of the harmonic and ripple content of the detected signal, is proposed in [55]. This shows that the synchronization based on PLLs and RDFTs requires less computational burden but the reliability can be increased by using a DKF.

An improvement of the estimation of the grid parameters, in terms of accuracy and speed can be obtained by using the strategy proposed in [26]; this is based on the idea of considering two separate methods: one for the frequency tracking and the other for the phase angle and amplitude estimation. The first is a method based on modulating functions [47]; its grid frequency estimation is used to adjust the resonance frequency of the SOGI, and in this way the transients are reduced and the signal parameters estimation is improved. Therefore, besides a considerable simplification of the PLL structure, the strategy presents the advantages of a fast and accurate signal tracking capability and a good rejection to noise due to the low-pass filter properties of the modulating functions. The idea of considering separate methods for frequency, amplitude, and phase is not new. For example, in [21], an adaptive PLL scheme is proposed based on three feedback control units one for each parameter to estimate. As the same author says, it does not exist a generic control design approach for this kind of PLL system, since it is a multivariable adaptive nonlinear and it could be difficult to investigate theoretically. The aim of this chapter is to provide new contributions in terms of clarification on the state of the art of simple single-phase approach for frequency, amplitude, and phase estimation.Moreover a new estimation method, already proposed in [26] is presented. The advantages of the proposed strategy and detailed description of the signal tracking method based on modulating functions will be presented. Finally the chapter proposes the presentation of some laboratory results obtained, in particular, some comparisons are reported in terms of accuracy of frequency estimation with the PLLs proposed in [32] and in [36] and with RDFT proposed in [3].

1.2 PLL structure for grid-connected systems

The recent increasing interest in PLL topologies for grid-connected systems has led to the proposal of the general structure shown in

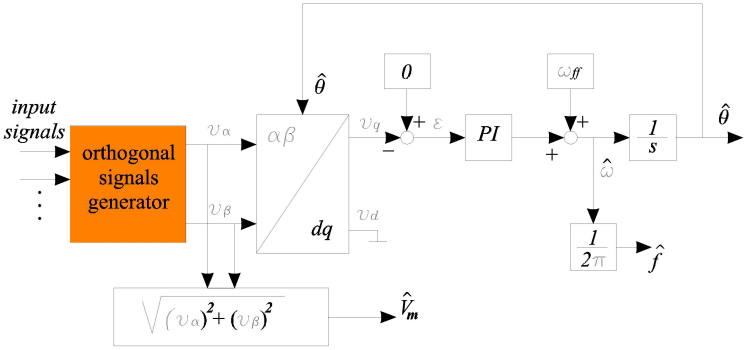

Fig. 1.1. General structure of PLL topology.

Fig. 1.1. It can be specified for three-phase PLL, if the input signals are the three utility voltages and for single-phase PLL if the single input signal is the grid voltage.

In any case, this PLL topology includes an orthogonal signals generator (OSG) and a feedback control system, providing the estimations $\hat{\theta}$ and $\hat{\omega}$ of the utility phase θ and the utility angular frequency ω respectively. The task of the OSG is to generate two orthogonal signals v_α and v_β, closely synchronized with the input signals:

$$\begin{aligned} v_\alpha &= V_m sin\theta, \\ v_\beta &= -V_m cos\theta \end{aligned} \tag{1.1}$$

where $\theta = \omega t + \phi$.

As shown in Fig. 1.1, the orthogonal signals v_α and v_β are the inputs of a Park transformation, whose rotating matrix depends on estimation $\hat{\theta}$. In particular, choosing such a matrix as:

$$T\left(\hat{\theta}\right) = \begin{bmatrix} cos\hat{\theta} & sin\hat{\theta} \\ -sin\hat{\theta} & cos\hat{\theta} \end{bmatrix}$$

and taking into account (2.4), the component v_q is derived as:

$$v_q = V_m sin(\theta - \hat{\theta}). \tag{1.2}$$

Therefore, setting the reference value of v_q equal to zero and assuming that the phase difference $\theta - \hat{\theta}$ is very small, the PLL output $\hat{\theta}$ can track the phase of the utility voltage by the proper design of the proportional-integral (PI) loop filter. In addition, the estimations of the frequency $\hat{f} = \hat{\omega}/2\pi$ and the amplitude of the utility voltage $\hat{V}_m = \sqrt{v_\alpha^2 + v_\beta^2}$ are also determined (see Fig. 1.1). The feed-forward frequency command ω_{ff} is introduced to improve the overall tracking performance of the PLL. There are various methods to design the loop filter. The second-order loop is commonly used as good trade-off between the filter performance and system stability. In particular, a low dynamic filter will produce a very filtered and stable output but with a longer synchronization time; on the other hand, a design for fast dynamics will produce an output which is able to synchronize to the input quickly, but distortions in the input signal will pass through the filter and become part of the output signal. Tuning methods for the gains associated with the PI filter are described in [25],[29], [1], [30]. Moreover, it is worth pointing out that the choice of ω_{ff} requires the assumption of a-priori knowledge of the frequency range of the input signal.

As already explained, an essential element of the PLL structure of Fig. 1.1 is the OSG. In a three phase system the orthogonal reference signals can be obtained by the Clarke transformation. However, under unbalanced utility voltage, the Clarke transformation can be applied only by separating the positive and negative sequences present in the voltages and by feeding back only the positive sequence [25],[29],[53],[7],[30]. In a single-phase system, to overcome the problem due to the available information, which is less than the three-phase system one regarding the grid condition, there is an increasing number of proposed methods to create an orthogonal voltage system. An easy way of generating the orthogonal voltage system in a single-phase structure is using a transport

delay block, which is responsible for introducing a phase shift of 90 degrees with respect to the fundamental frequency of the input signal equal to the grid voltage. A more complex method of creating a quadrature signal is using the Hilbert transformation. Another method to generate the orthogonal signals consists in the use of an inverse Park transformation, whose rotating matrix also depends on estimation $\hat{\theta}$. However, these methods have one or more of the following shortcomings: frequency dependency, high complexity, nonlinearity, poor or none filtering [29], [54], [53],[33]. An alternative of creating an orthogonal voltage system for a single-phase consists in using a SOGI [34],[32].

1.2.1 The OSG based on SOGI

The block diagram of the OSG based on SOGI (OSG-SOGI) is depicted in Fig. 1.2. The input signal v of the OSG is the grid voltage, while the SOGI requires an angular frequency ω_r as input. Obviously, the output signals of the OSG are the two orthogonal signals v_α and v_β.

The two closed-loop transfer functions of the structure in Fig. 1.2 are:

$$H_\alpha(s) = \frac{V_\alpha(s)}{V(s)} = \frac{A\omega_r s}{s^2 + A\omega_r s + \omega_r^2}, \tag{1.3}$$

$$H_\beta(s) = \frac{V_\beta(s)}{V(s)} = \frac{A\omega_r^2}{s^2 + A\omega_r s + \omega_r^2}. \tag{1.4}$$

It is easy to observe that these functions represent two second-order filters with a bandwidth affected by the gain A and a resonance angular frequency equal to ω_r. This is well highlighted in the Bode diagrams shown in Fig. 1.3; they refer to the two functions $H_\alpha(s)$ and $H_\beta(s)$ with different values of gain A.

As it can be seen from Fig. 1.3(a), at the resonance frequency there is no attenuation and the phase is equal to zero; instead, there is a quite large attenuation outside the resonance frequency and moreover, if A decreases the bandwidth of the filter becomes narrower resulting a heavy filtering. As a consequence, if the grid

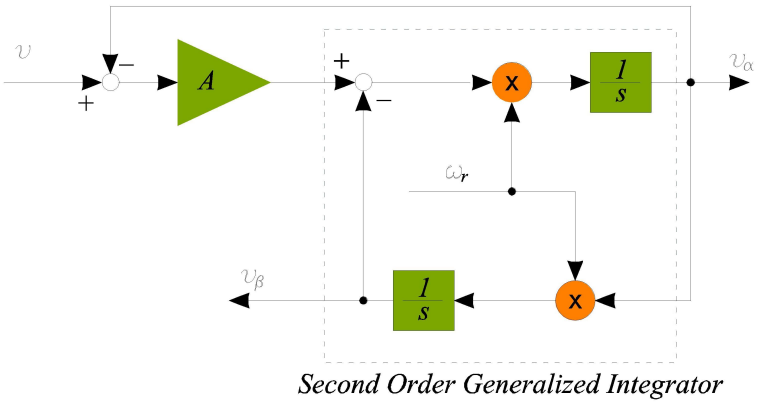

Fig. 1.2. OSG based on SOGI.

frequency ω is equal to the resonance frequency ω_r, the input grid voltage v is filtered and then the signal v_α has the same phase and magnitude as the fundamental of the input signal. As clearly shown in Fig. 1.3(b), the second function represents a second-order low-pass filter, with static gain A and damping coefficient $A/2$; so it has no attenuation and phase equal to -90^o at the resonance frequency ω_r. Thus, if the grid frequency is at the resonance frequency of the SOGI, the signal v_β is a clean voltage orthogonal to v_α.

The OSG-SOGI method, as it can seen from Fig. 1.2, uses a simple structure to generate two clean orthogonal voltage waveforms having the significant advantage of a filtering without phase delay; as it is well known, using filtering, generally delays will be introduced in the signals which are unacceptable in the case of grid voltage angle. As it is already said, the OSG-SOGI structure requires an adaptive tuning with respect to its resonance frequency. This can be achieved by adjusting the resonance frequency of the SOGI online using the frequency provided by the feedback con-

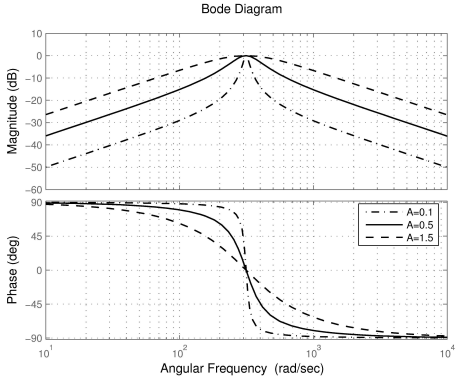

(a)

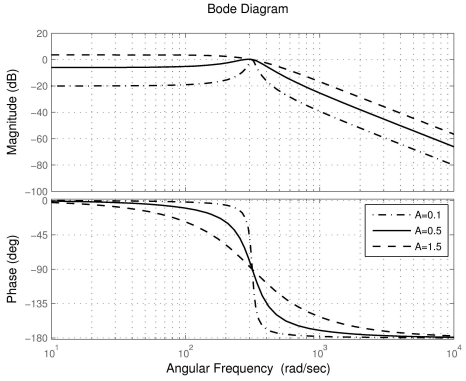

(b)

Fig. 1.3. Bode diagram of the functions: a) $H_\alpha(s)$ and b) $H_\beta(s)$ for different values of gain A.

trol loop of the PLL structure; however, in this way, the behavior of the whole PLL structure will be affected by the transients of the OSG-SOGI and the feedback control loop. Moreover, the

OSG-SOGI structure has the drawback, common to other known methods, of being sensitive to grid voltage offset. Indeed, as it can be seen from the Bode diagrams in Fig. 1.3, the structure rejects the eventual dc component of the grid voltage only for the signal v_α; instead, the signal v_β is directly affected by a dc component equal to the voltage offset multiplied gain A. On the other hand, the voltage offset is often produced in the measurements and data conversion processes; then, without providing offset rejection solutions, there will be a malfunction of the OSG-SOGI structure and consequently significant errors for the estimated parameters of the grid voltage will be provided by the PLL technique. Recently, a simple offset rejection method has been proposed in [32]; it just aims to correct the signal v_β, eliminating its dc component, so that the feedback control system of the PLL can operate with two clean orthogonal input waveforms both without offset. This solution makes the OSG-SOGI structure slightly more complex, because it requires an additional low pass filter in order to filter out the harmonics which can be present in the grid voltage v.

1.3 Signal Tracking Strategy Proposed

The signal tracking strategy proposed has in common with the PLL topology of Fig. **??** only the OSG-SOGI structure, because it does not need the feedback control loop. The basic idea of the strategy is to consider two separate methods: one for tracking the frequency and the other for estimating the phase and amplitude. The diagram scheme of the proposed strategy is shown in Fig. 1.3. The block denoted as FT is to represent a frequency tracking method, that provides a grid frequency estimation; this value is also used to adjust the resonance frequency of the OSG-SOGI structure, whose output are thus two clean orthogonal signals v_α and v_β.

The information about the amplitude and the phase of the grid signal is obtained by means of simple operations on the output signals of the SOGI; in particular, considering the expressions

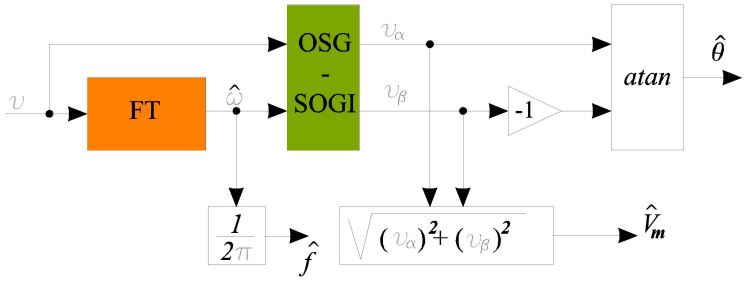

Fig. 1.4. Diagram scheme of the proposed strategy.

(2.4) the estimations are derived as :

$$\begin{aligned} \hat{\theta} &= atan(-v_\alpha / v_\beta), \\ \hat{V}_m &= \sqrt{v_\alpha^2 + v_\beta^2}. \end{aligned} \tag{1.5}$$

Besides a considerable simplification of the whole structure compared with that of the PLL topology, the proposed strategy presents the advantages of a fast and accurate signal tracking capability and a good rejection to noise due to the low-pass filter properties of the frequency tracking method. Moreover, since the frequency tracking method has also the property of not being sensitive to the grid offset voltage, then the proposed strategy has the advantage to leave unchanged the tuning of the OSG-SOGI structure, even when a dc component is present in the grid voltage. Of course, in order to obtain the correct estimations of the phase and amplitude, it is necessary to consider in (1.5) a signal v_β without dc component; this can be achieved by using the same solution proposed in [32]. A frequency tracking method having the above desired properties is that based on the modulating functions. This method will be explained in the next section.

1.4 Frequency tracking method based on modulating functions

A function $\phi_K(t) \in C^K$ (K-times differentiable), defined over a finite time interval $[0, T]$, which satisfies the following terminal conditions:

$$\phi_K^{(i)}(0) = \phi_K^{(i)}(T) = 0, \quad \forall i = 0, 1, ..., K-1, \tag{1.6}$$

is called modulating function [47]. A function $f(t) \in L^1$ over $[0, T]$ is modulated by taking the inner product with a modulating function $\phi_K(t)$:

$$\langle f, \phi_K \rangle = \int_0^T f(t)\phi_K(t)dt. \tag{1.7}$$

The terminal constraints of eq. (1.6) essentially make the boundary conditions of the function $f(t)$ irrelevant after modulations. Moreover, they make possible the transfer of the differentiation operation from the function $f(t)$ on to the modulating function $\phi_K(t)$. Indeed, according to (1.7), the ith derivative of function $f(t)$ is modulated by considering the following expression:

$$\langle f^{(i)}, \phi_K \rangle = \int_0^T f^{(i)}(t)\phi_K(t)dt. \tag{1.8}$$

By means of the integration by parts and the terminal conditions, it is possible to obtain:

$$\langle f^{(i)}, \phi_K \rangle = (-1)^i \langle f, \phi_K^{(i)} \rangle, \quad i = 0, 1, ..., K-1. \tag{1.9}$$

This result is very useful, because it eliminates the need to approximate time derivatives from noisy measurement data. The modulating functions implemented in the paper are of spline type and they are shown in Fig. 1.4. Briefly, the class of spline functions is characterized by two parameters: the order K of the highest derivative of $\phi_K(t)$, and the characteristic time $\bar{T}$; for a function

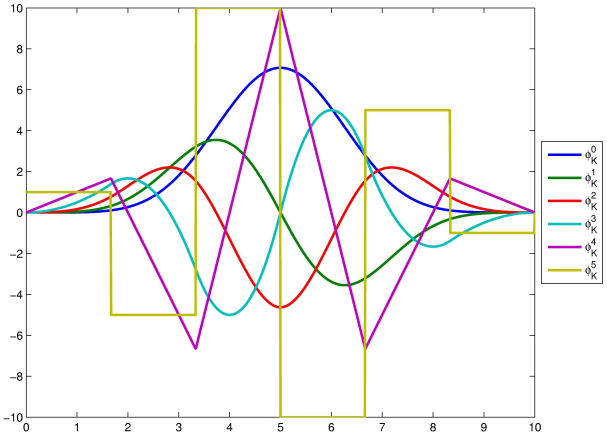

Fig. 1.5. Spline function with $K = 6$ and $T = 10$s.

$\phi_K(t)$, defined into the interval $[0, T]$, $\bar{T} = T/K$. The ith derivative of a spline function, with order K and characteristic time $\bar{T}$, is expressed as

$$\phi_K^{(i)}(t) = \begin{cases} \sum_{j=0}^{K} (-1)^j \binom{K}{j} g_{ji}(t - j\bar{T}),\ i = 0, 1, ..., K-1, \\ \sum_{j=0}^{K} (-1)^j \binom{K}{j} \delta(t - j\bar{T}), \quad i = K, \end{cases} \tag{1.10}$$

where

$$g_{ji}(t - j\bar{T}) = \begin{cases} \frac{1}{(K-i-1)!}(t - j\bar{T})^{K-i-1},\ t \in [j\bar{T}, T], \\ 0, \qquad\qquad\qquad \text{otherwise}, \end{cases} \tag{1.11}$$

and $\delta(t)$ is the Dirac delta function.

Consider a signal $v(t)$ equal to the sum of a sinusoidal signal and a dc component:

$$v(t) = A_0 + A\sin(\omega t + \phi), \tag{1.12}$$

it is effortless to verify that

$$v^{(3)}(t) + \rho v^{(1)}(t) = 0 \tag{1.13}$$

where $\rho = \omega^2$. The last equation can be used to get an estimation $\hat{\rho}$ of the parameter ρ and then of the angular frequency of the sinusoidal signal; note that the dc component is not included in (1.13) so that the consequent estimation procedure is not sensitive to the signal offset. The modulation with the modulating functions permits to convert (1.13) into an algebraic equation with the same mathematical form as follows:

$$\int_0^T \phi_K(t) v^{(3)}(t) dt + \rho \int_0^T \phi_K(t) v^{(1)}(t) dt = 0. \tag{1.14}$$

Integrating by parts and using the terminal conditions (1.6), (1.14) becomes

$$\int_0^T \phi_K^{(3)}(t) v(t) dt + \rho \int_0^T \phi_K^{(1)}(t) v(t) dt = 0. \tag{1.15}$$

Since in the previous equation, the 3rd order derivative of $\phi_K(t)$ is involved, then the order K must be greater or equal to 4. The foregoing procedure has the primary advantages of involving the known derivatives of the modulating functions instead of the derivatives of the usually noisy output data $v(t)$. Furthermore, since the modulating function approach is an integral method, it has low-pass filter properties and then it is able to mitigate the components of the signal with frequency greater than the cut-off frequency, proportional to $1/T$ [27]. For such reason, in the presented analysis, the noise and harmonic contribution can be omitted, but their effects will be considered in the experiments section.

Consider a moving data window $W_{(m)}$ of n continuously arriving data of the signal $v(t)$ sampled with a period T_s such that $T = (n-1)T_s$:

$$\begin{aligned} W_{(m)} = &\left[v(mT_s), v((m+1)T_s), ..., v((n+m-1)T_s)\right], \\ &m = 0, 1, ... \end{aligned} \tag{1.16}$$

and define the following quantities

$$\begin{aligned} v_{1_{(m)}} &= \sum_{j=0}^{n-1} v((m+j)T_s)\phi_K^{(1)}(jT_s), \\ v_{3_{(m)}} &= -\sum_{j=0}^{n-1} v((m+j)T_s)\phi_K^{(3)}(jT_s). \end{aligned} \tag{1.17}$$

Note that $v_{1_{(m)}}T_s$ and $-v_{3_{(m)}}T_s$ represent approximations of the integrals involved in (1.15). As a consequence, (1.13) can be approximated by the following:

$$v_{3_{(m)}} - \hat{\rho}_h v_{1_{(m)}} = 0 \tag{1.18}$$

where h is the generic step; then the estimation problem becomes the determination of estimation $\hat{\rho}_h$ so as to minimize the following index

$$J_h = \frac{1}{2}\sum_{m=0}^{h} \mu^{h-m}\left[v_{3_{(m)}} - \hat{\rho}_h v_{1_{(m)}}\right]^2, \quad h = 0, 1, ... \tag{1.19}$$

The parameter μ is a positive constant in the interval $(0, 1]$ and represents a forgetting factor to exponentially discard the "old" data in the recursive scheme. This means that in the estimation process, the old measures have a weight smaller than that of the most recent measurements. The value of $\hat{\rho}_h$, which minimizes the index (1.19), is obtained by seeking the value that cancels $\partial J_h/\partial\hat{\rho}_h$; therefore, it is equal to:

$$\hat{\rho}_h = \frac{\sum_{m=0}^{h} \mu^{h-m} v_{1_{(m)}} v_{3_{(m)}}}{\sum_{m=0}^{h} \mu^{h-m} v_{1_{(m)}}^2}, \quad h = 0, 1, ... \tag{1.20}$$

A recursive algorithm of (1.20) is based on the following update law:

$$\hat{\rho}_{h+1} = \frac{1}{\alpha_{h+1}}\left(\mu\alpha_h\hat{\rho}_k + \beta_{h+1}\right), \quad h = 0, 1, ... \tag{1.21}$$

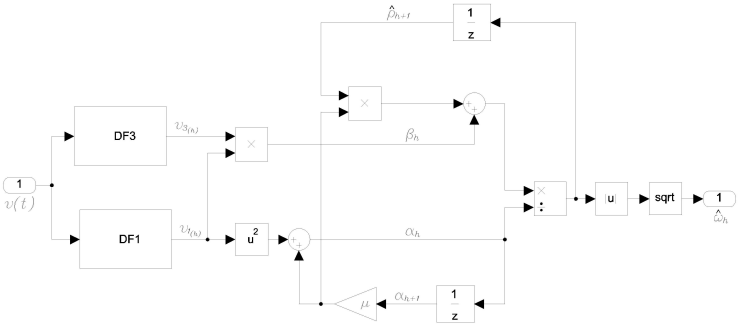

Fig. 1.6. MFFT Simulink diagram.

where

$$\begin{aligned} \alpha_h &= \sum_{m=0}^{h} \mu^{h-m} v_{1_{(m)}}^2, \\ \beta_h &= v_{1_{(h)}} v_{3_{(h)}}, \qquad h = 0, 1, ... \end{aligned} \tag{1.22}$$

Note that α_{h+1} can be recursively calculated by using

$$\alpha_{h+1} = \mu \alpha_h + v_{1_{(h+1)}}^2, \quad h = 0, 1, ... \tag{1.23}$$

In Fig. 1.6 the block diagram of the Modulating Functions Frequency Tracking (MFFT) method implemented in Matlab/Simulink is depicted. Such a diagram shows some interesting issues about the implementation of the proposed method. In particular, the two quantities $v_{1_{(m)}}$ and $v_{3_{(m)}}$ of (1.17) are obtained by the Matlab Digital Filter Blocks DF1 and DF3 respectively, where the filter coefficients have been substituted with the values of the derivatives of the Modulating Function $\phi_K^{(1)}(jT_s)$ and $\phi_K^{(3)}(jT_s)$, $j = 0, 1, ..., n-1$. This allows to quantify the computational burden of the MFFT method as about the same of that required for the implementation of two digital filters each having n coefficients.

Thus, according to the scheme depicted in Fig. 1.3, the proposed strategy consists in the combined use of the MFFT method and the OSG-SOGI (MFFT-OSG-SOGI), and it allows to improve

the noise reduction capability without deteriorating the performances in terms of speed estimation, compared with the other synchronization methods. Moreover, the estimation recursive algorithm with a forgetting factor is able to get a fast tracking in case of abrupt changes of the frequency of the signal $v(t)$. In this way, the proposed strategy guarantees that OSG-SOGI always operates with a resonance frequency near to the frequency of the input signal; it is worth to note that, differently from the method based on PLL structure, the MFFT-OSG-SOGI approach is able to track the unknown frequency of the signal without any a-priori assumption on the frequency range of the signal itself. As regards the problem of choosing the window length or the forgetting factor value, it is reasonable to think that increasing the window length (i.e. the number of points in the window), the filter effect increases but the capability to track a signal decreases. Moreover decreasing the forgetting factor increases the dynamic capabilities of the method to track a signal which is varying. Clearly a correct choice is dependent by the particular application. It is worth to note, however, that the PLL-based methods suffer of similar drawbacks. Also in this case there are free parameters to correctly tune in order to avoid a deterioration of the performances. Moreover, any PLL-based method requires an a-priori knowledge about the frequency to track. Such a knowledge is necessary to decrease the transient of the synchronization system.

1.5 Experimental results

Some significant simulations experiments were already shown in [26], referred to two different situations: a not distorted input signal and a reference voltage signal distorted by adding a third harmonic of amplitude equal to 5% of the fundamental.

In this section, in order to investigate the effectiveness of the proposed method, some new simulated and laboratory experiments are presented. Moreover, for an easier evaluation of both

advantages and drawbacks of the presented approach, a comparison with the PLL topology proposed in [34], namely SOGI-PLL, with the QPLL proposed in [36] and with the RDFT method proposed in [3] is provided.

The methods were tested using National Instruments DAQPad-6015 Acquisition Board (AB) and Agilent 33120A Arbitrary Waveform Generator (AWG) in order to generate the testing signals. Both AB and AWG were interfaced and controlled by a PC equipped with the Matlab software. In this way it has been possible to examine a wide range of grid voltage conditions, including step and sweep changes in frequency as well as amplitude variations. In particular, with the intent to put in evidence the robustness of the MFFT-OSG-SOGI, the experiments were conducted producing by the AWG a voltage signal which contains $3rd$, $5th$ and $7th$ harmonics, each of amplitude equal to 5% of the fundamental, and gaussian white noises so as to obtain a Signal to Noise Ratio equal to 40dB.

All the results consider for the PI loop filter of the SOGI-PLL method the following controller parameters: the settling time $T_{set} = 0.06$s and the damping factor $\delta = 1$. The parameters of the QPLL were chosen as follows: $\mu_s = 100$, $\mu_c = 100$, $\mu_f = 100$, $K_c = 40$, $K_s = 40$. As regards the MFFT-OSG-SOGI strategy, a moving data window of $n = 400$ samples and a forgetting factor $\mu = 0.98$ were used. For both SOGI-PLL and MFFT-OSG-SOGI methods, the gain A of SOGI was chosen equal to 0.8. Moreover, all results were obtained without using additional output filters.

The first experiment deals with a frequency step from 47 to 52 Hz which are the frequency variation limits defined in UNE-EN 50160 and in UNE-EN 6000-2-4. As it can be seen from Fig. 1.7, the frequency estimation provided by the MFFT-OSG-SOGI method reaches the correct value with a satisfactory precision and with a similar time delay of the SOGI-PLL and the QPLL.

Fig. 1.8 shows the results for a frequency sweep from 50 up to 51 Hz. It starts about at 0.45s and goes up with slope of 10 Hz/s. Also in this case, the proposed method gives an estimation which

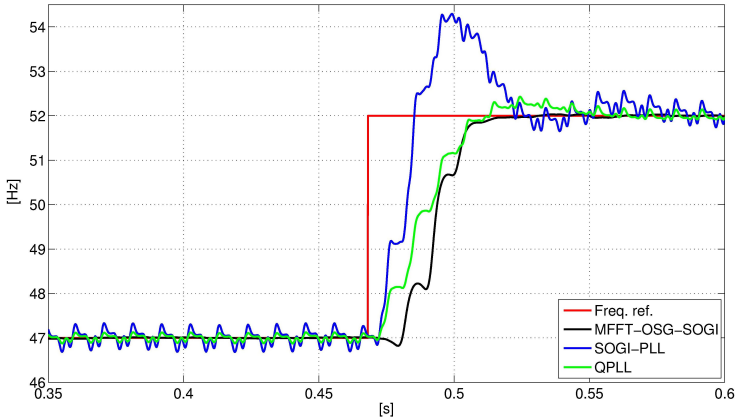

Fig. 1.7. Frequency tracking in the case of frequency step.

is robust with respect to the harmonic and the noise content of the input signal.

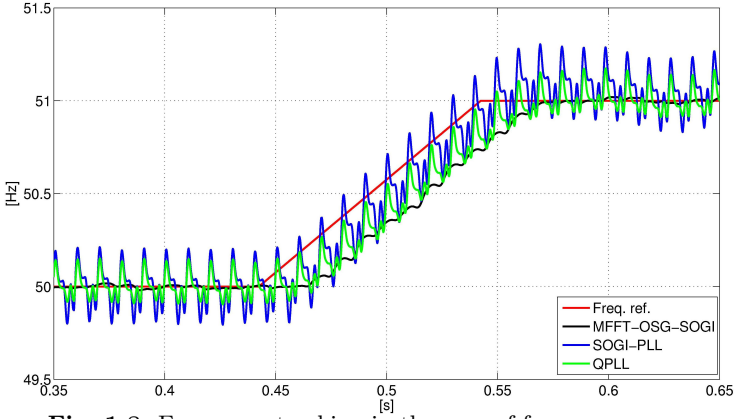

Fig. 1.8. Frequency tracking in the case of frequency sweep.

The third experiment refers to the presence of a voltage sag condition; in particular, the fundamental amplitude of the input signal decreases from a value of 1 V to 0.6 V. As clearly shown in Fig. 1.9, the amplitude estimations provided by the three methods are very similar.

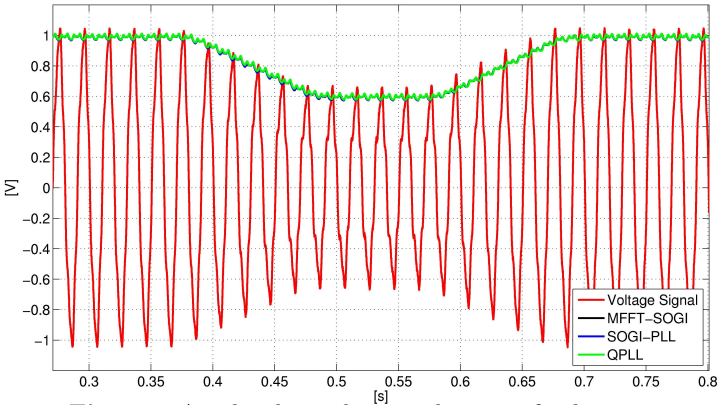

Fig. 1.9. Amplitude tracking in the case of voltage sag.

Another interesting comparison (shown in in Figs 1.10 and 1.11) has been carried out with the method proposed in [3]. In such a comparison a time window of 20ms containing 200 samples has been used for RDFT.

The experiment presented in Fig. 1.10 refers to the the estimation of the fundamental component of the input signal. As the figure shows, the performances provided by the two methods are comparable.

The experiment illustrated in Fig. 1.11 refers to the the estimation of the frequency of the input signal provided by the two methods. This experiment highlights the accuracy of the frequency estimation provided by MMFT method with respect to RDFT one.

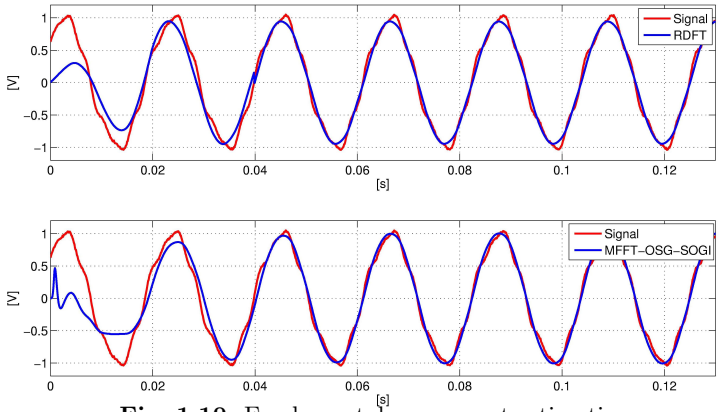

Fig. 1.10. Fundamental component estimation.

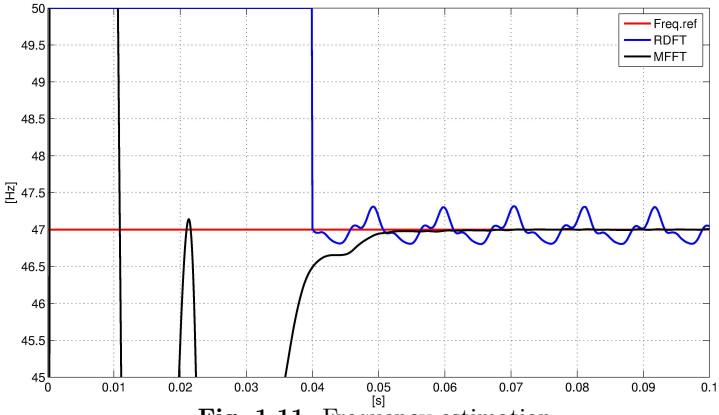

Fig. 1.11. Frequency estimation.

1.6 Conclusion

In this chapter many single-phase approach for frequency, amplitude, and phase estimation have been presented and compared with a proposed strategy for the signal tracking in EPSs. The basic idea is the combined use of the modulating functions method to

estimate the frequency of the signal and an orthogonal signals generation system, based on the second order generalized integrator, to estimate amplitude and phase of the signal. The convenience of the proposed strategy derives from the consideration that the frequency estimation method, based on modulating functions, can adjust the value of the SOGI resonance frequency and it is able to lock the unknown signal without any a-priori assumption on the frequency range of the signal. Experiments conducted in highly distorted environment proved the good capability and robustness of the proposed strategy.

2

New concept in electrical power systems analysis

This chapter presents a new approach to model the electrical signals in power systems. The approach is based on the concept, derived from differential geometry, of contact between a signal and an osculating sinusoid. A direct application leads to a synchronization algorithm performing tasks comparable to those of single-phase PLL as verified by some different simulation results. Moreover, a significant advantage of the approach is the possibility to define quantities typically considered in sinusoidal steady state conditions also during the transients.

A difficulty in applying the approach lies in the calculation of the osculating sinusoid parameters, when the signal contains noise. In order to overcome this problem, this chapter deals with a computation algorithm for determining the osculating sinusoid parameters also in presence of noise on the signal. Accordingly, a new method providing a fast and accurate estimation of the frequency, phase and amplitude for noisy grid signals is developed. The good performance of the method is verified by some significant simulation results.

2.1 Introduction

Many of the concepts used in power systems analysis have been historically developed under the assumption of steady state operations. In particular, the definitions of the power flows and the characterization of the grid voltages and currents are based on indexes and parameters (THD, rms value, etc.), that can be strictly defined only in the steady state condition. However, the need to treat transient phenomena is a key issue in the actual power systems, especially considering the increase of equipments based on power electronic converters, connected to the grid, such as UPS, Shunt and Series Compensator (SC) and DG systems [46], [8].

The use of static converters allowing quick responses to variations in the utility grid, is very effective to correct or avoid problems and bad operating modes. However, for a correct operation in grid connected condition, the static converters continuously need information on amplitude, phase angle and frequency, etc., of the grid voltages and currents, also during the transient period. Considering the capacity of SCs and DG systems to operate services as power management or voltage control at the distribution level, it is important to develop new approaches able to represent grid voltages and currents both in the steady state conditions as well in the transient ones. Thus, as already explained in the previous chapter, many estimation and synchronization methods, like suitable PLL algorithms, have been recently developed and proposed to obtain informations about the aforesaid parameters both in the steady state and during the transient periods [29], [34]. However, the main aim of these synchronization methods is to simply track the evolution of grid parameters like frequency or voltage amplitude, without giving them any meaning during the transients.

This chapter presents a new modeling approach for electrical signals in power systems which is based on the concept, derived from the differential geometry, of contact at an instant between a signal and an osculating sinusoid. As it will be explained, just by realizing this match for every instant of time, a generic signal can be modeled by a sinusoidal signal of amplitude, angular frequency

and phase variable at every instant of time. This point of view allows to extend the same concepts, used in steady state conditions to characterize the grid signals, also in the transient operation. In order to prove the effectiveness of the proposed modeling approach, the chapter contains some different simulation results about its direct application as synchronization algorithm able to give fast and accurate estimations of the amplitude, frequency and phase angle of the grid signals.

2.2 p-q Theory

The definitions of some instantaneous quantities that will be provided, by the proposed approach, in the following sections, can be considered as an alternative formulation with respect to the instantaneous power theory or *p-q Theory*. This theory, proposed by Akagy et al. in 1983, is widely used in the same application field of the proposed modeling approach. Then, knowing the importance obtained by the Akagy's approach in the lasts few decades, this section aims to provide a brief description of the aforementioned theory.

As known from the literature [15], [16], the *p-q Theory* defines a set of instantaneous powers in the time domain. Since no restrictions are imposed on voltage or current behaviors, it is applicable to three-phase systems of generic voltage and current waveforms; thus it is valid not only in steady states, but also during transient states.

This theory deal with the three phases of a three-phase system as a sole system, not as a superposition or sum of three single-phase circuits. It uses the $\alpha\beta 0$-transformation, known as the Clarke Transformation, which consists of a real matrix that transforms three-phase voltages and currents into the $\alpha\beta 0$-stationary reference frame.

Then, given a set of three-phase instantaneous voltages $v_a(t)$, $v_b(t)$ and $v_c(t)$, the Clarke transformation is given by

$$\begin{bmatrix} v_0(t) \\ v_\alpha(t) \\ v_\beta(t) \end{bmatrix} = \sqrt{\frac{2}{3}} \begin{bmatrix} \frac{1}{\sqrt{2}} & \frac{1}{\sqrt{2}} & \frac{1}{\sqrt{2}} \\ 1 & -\frac{1}{2} & -\frac{1}{2} \\ 0 & \frac{\sqrt{3}}{2} & \frac{\sqrt{3}}{2} \end{bmatrix} \begin{bmatrix} v_a(t) \\ v_b(t) \\ v_c(t) \end{bmatrix} \tag{2.1}$$

In a similar way, three-phase generic instantaneous line currents $i_a(t)$, $i_b(t)$ and $i_c(t)$, can be transformed on the three-phase orthogonal system $\alpha\beta 0$ by

$$\begin{bmatrix} i_0(t) \\ i_\alpha(t) \\ i_\beta(t) \end{bmatrix} = \sqrt{\frac{2}{3}} \begin{bmatrix} \frac{1}{\sqrt{2}} & \frac{1}{\sqrt{2}} & \frac{1}{\sqrt{2}} \\ 1 & -\frac{1}{2} & -\frac{1}{2} \\ 0 & \frac{\sqrt{3}}{2} & \frac{\sqrt{3}}{2} \end{bmatrix} \begin{bmatrix} i_a(t) \\ i_b(t) \\ i_c(t) \end{bmatrix} \tag{2.2}$$

If zero-sequence components are not present on the three-phase currents and voltages both the components i_0 and v_0 are equal to zero. Moreover α-axis and β-axis components are not affected by zero-sequence components. In particular, when zero-sequence components are not present in both the currents and voltages of a three-phase circuit the *p-q Theory* suggest to characterize the powers flowing through the circuit according to the following relationships:

$$\begin{bmatrix} p(t) \\ q(t) \end{bmatrix} = \begin{bmatrix} v_\alpha(t) & v_\beta(t) \\ -v_\beta(t) & v_\alpha(t) \end{bmatrix} \begin{bmatrix} i_\alpha(t) \\ i_\beta(t) \end{bmatrix} \tag{2.3}$$

where $p(t)$ is defined as instantaneous real power and $q(t)$ is the instantaneous imaginary power. In a balanced three-phase system, where only direct-sequences are present in currents and voltages, $p(t)$ and $q(t)$ are constant and equal to the three-phase conventional active power and reactive power respectively. Note that this last hypothesis involves sinusoidal stationary conditions. However,

as already said, the definition of $p(t)$ and $q(t)$ can be applied in steady-state as well as during transients and, under the assumption of balanced system, the *p-q Theory* provides a very efficient and flexible basis for designing control strategies aiming to impose desired instantaneous powers p^* and q^*. These strategies was implemented in the form of controllers for power conditioners based on power electronics devices [44],[31].

However, the hypothesis of balanced and symmetrical system represents a really strict constrain that limits the possibility of application of the *p-q Theory* so as defined in (2.3). For a three-phase four-wire system, when the power system is unbalanced or distorted, the use of (2.3) alone, involves the unacceptable cancellation of the zero-sequence components. Thus, 0-axis current and voltage components have to be considered, resulting in a growth of complexity which decreases the benefits, in terms of effectiveness and flexibility, in the use of the *p-q Theory*.

Moreover, as suggested in [4], this theory misinterprets power properties of electrical systems or provides some results that at least defy a common sense or meaning of some notions in electrical engineering. For example, it suggests the presence of an instantaneous reactive current in supply lines of purely resistive loads and the presence of an instantaneous active current in supply lines of purely reactive loads. Moreover, it suggests that line currents of linear loads with sinusoidal supply voltage contain a non-sinusoidal component.

Moreover, it is worth to underline that *p-q Theory* is applicable only for three-phase systems being the Clarke transformation an important and irreplaceable part of the approach.

However, it is beyond doubt that, the *p-q Theory* is one of the most important approach to deal with transients in EPSs and, in spite of the numbers or drawbacks occurring under not ideal conditions, it is widely used especially to design power converter control systems. In particular can be said that, its diffusion proves the importance of the development of methods able to face transient phenomena for power systems applications.

2.3 The proposed modeling approach

The proposed modeling approach is based on the concept of contact between two curves on R^2 in differential geometry.

In particular, consider two curves on R^2 described by the real functions $y = f(x)$ and $y = g(x)$ continuous and with continuous derivatives up to an order of interest and suppose they go to a point P of abscissa x_0 ; if it occurs that at the point P, the two functions and their derivatives up the order n have the same values, whereas the derivatives of order $n + 1$ are different i.e.:

$$\begin{gathered} f(x_0) = g(x_0), \quad f^{(1)}(x_0) = g^{(1)}(x_0), \quad ..... \\ f^{(n)}(x_0) = g^{(n)}(x_0), \quad f^{(n+1)}(x_0) \neq g^{(n+1)}(x_0). \end{gathered} \tag{2.4}$$

it is said that the two curves have a n-th order contact at point P . A zero order contact means that the curves have a simple crossing at P, a first order contact corresponds to two curves tangent at P and two curves having a second order contact are said osculating.

As known in differential geometry, the osculating circle of a curve at a point is just a circle having a second order contact (at least) with the curve at that point. The three conditions obtained by (2.4) specified with n=2, define a unique osculating circle for each point on the curve, provided that the second derivative is not zero. Indeed, for each value x_0 , the three conditions, defining the second order contact, give three equations in the three unknown quantities of the osculating circle: radius and coordinates of the center.

In a similar way, for a generic electrical signal $y(t)$ it is possible to define as osculating sinusoid of $y(t)$ at instant t_0 , the signal $s(t)$ given by:

$$s(t) = Y_0 \sin \theta(t) \quad \text{whith} \quad \theta(t) = \omega_0 t + \varphi_0. \tag{2.5}$$

and meeting the following conditions:

$$s(t_0) = y(t_0), \quad s^{(1)}(t_0) = y^{(1)}(t_0), \quad s^{(2)}(t_0) = y^{(2)}(t_0). \tag{2.6}$$

i.e. satisfying the three equations:

$$Y_0 \sin\theta(t_0) = y(t_0), \tag{2.7}$$

$$\omega_0 Y_0 \cos\theta(t_0) = y^{(1)}(t_0), \tag{2.8}$$

$$\omega_0^2 Y_0 \sin\theta(t_0) = -y^{(2)}(t_0). \tag{2.9}$$

Through simple manipulations, the following solutions can be obtained:

$$\omega_0 = \sqrt{-\frac{y^{(2)}(t_0)}{y(t_0)}}, \tag{2.10}$$

$$\theta(t_0) = \arctan\left[\frac{\sqrt{-y^{(2)}(t_0)y(t_0)}}{y^{(1)}(t_0)}\right], \tag{2.11}$$

$$Y_0 = \sqrt{[y(t_0)]^2 + \left[y^{(1)}(t_0)/\omega_0\right]^2}. \tag{2.12}$$

It is easy to observe that the angular frequency given by (2.10) is not real when the following condition is verified:

$$y^{(2)}(t_0)/y(t_0) > 0. \tag{2.13}$$

this impose to define the osculating sinusoid, substituting (2.14) with the equation:

$$\omega_0^2 \sin\theta(t_0) = \text{sign}\left[\frac{y^{(2)}(t_0)}{y(t_0)}\right] y^{(2)}(t_0). \tag{2.14}$$

so that the angular frequency is determined by:

$$\omega_0 = \sqrt{\left|y^{(2)}(t_0)/y(t_0)\right|}, \tag{2.15}$$

and analogously the instantaneous value of the phase-angle $\theta(t_0)$ will be obtained by using:

$$\theta(t_0) = \arctan\left[\frac{\sqrt{\left|y^{(2)}(t_0)y(t_0)\right|}}{y^{(1)}(t_0)}\right], \tag{2.16}$$

In this way, it is always possible to define the signal $s(t)$, given by (2.5); it will still be called osculating sinusoid, but it actually has a second order contact with $y(t)$ at t0 only when condition (2.13) doesnt occur. Then, once determined the parameters ω_0, $\theta(t_0)$ and Y_0 , the value of $y(t)$ at the instant t_0 can be seen as obtained by its osculating sinusoid evaluated at the same instant t_0 .

In order to better clarify the peculiarities of the modeling approach, we consider to apply it to the signal $y(t) = t^3 e^{-t}$. By using (2.15), (2.11) and (2.12), it is possible to determine the osculating sinusoids practically for every instant. Fig. 2.3 shows the signal to be represented and the osculating sinusoids in two different instants.

Then, assuming to make the match between the signal $y(t)$ and its osculating sinusoid for every instant of time, we can say that the signal $y(t)$ can be represented in the following way:

$$y(t) = Y(t)\sin\theta(t) \quad \text{whith} \quad \theta(t) = \omega(t)t + \varphi(t) \tag{2.17}$$

that means, the signal $y(t)$ can be seen as a sinusoidal signal of amplitude, angular frequency and phase variable at every instant of time.

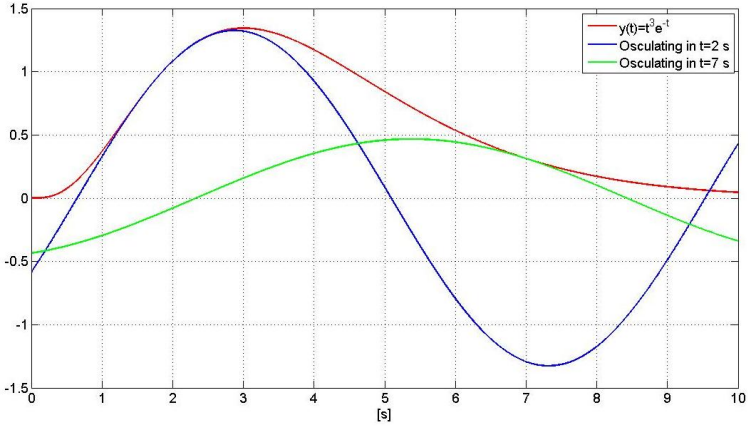

Fig. 2.1. "Osculating sinusoids" of $y(t) = t^3 e^{-t}$ for $t = 2$s and $t = 7$s

Clearly, when $y(t)$ is just a sinusoidal signal, it is exactly represented by (2.17), in which the amplitude $Y(t)$, the angular frequency $\omega(t)$ and the phase $\varphi(t)$ are constant. On the other hand, it is worth observing that the power electrical signals, to which the modeling approach is applied, are generally characterized by waveforms, that converge to sinusoidal signals of grid frequency.

2.3.1 Calculation of the Osculating Sinusoids Parameters

From equations (2.7), (2.8) and (2.14) it is easy to observe that, at the generic instant t_0 certainly there is an osculating sinusoid of finite angular frequency and not zero amplitude if we exclude the following cases:

$$\left\{y(t_0) = y^{(1)}(t_0) = y^{(2)}(t_0) = 0\right\} \vee \left\{y(t_0) = 0 \wedge \left[y^{(2)}(t_) \neq 0 \vee y^{(1)}(t) = 0\right]\right\}$$

Moreover, it is important to observe that (2.15) becomes undefined when $y(t_0) = y^{(2)}(t_0) = 0$, i.e when $\theta(t_0) = k\pi$, with $k = 0, 1, ...$ The undefined condition involves computational errors in the angular frequency estimation, because in this case is impossible to define a unique osculating sinusoid merely considering the three equations (2.7), (2.8) and (2.14). We consider then the further equation

$$y^{(3)}(t_0) = -\omega_0^3 \sin(\theta(t_0)) \tag{2.18}$$

so as to obtain the estimation of the angular frequency as:

$$\omega_0 = \sqrt{\left|y^{(3)}(t_0)/y^{(1)}(t_0)\right|}, \tag{2.19}$$

Clearly, this expression allows the correct estimation of ω_0 when $\theta(t_0) = k\pi$, but it gets undefined when $y^1(t_0) = y^3(t_0) = 0$, i.e. when $\theta(t_0) = (2k+1)\pi/2$ with $k = 0, 1, ...$ Then, combining the estimations of the angular frequency provided by the tow equations (2.15) and (2.19), and using the estimation of $\theta(t_0)$ provided by (2.16), a new relationship which provides the the correct value of the angular frequency avoiding computational error can be obtained, so as explained by the following algebraical manipulation:

$$\begin{aligned} \left|\frac{y^{(2)}(t_0)}{y(t_0)}\right| \sin^2\theta(t_0) + \left|\frac{y^{(3)}(t_0)}{y^{(1)}(t_0)}\right| \cos^2\theta(t_0) = \\ = \omega_0^2 \sin^2\theta(t_0) + \omega_0^2 \cos^2\theta(t_0) = \omega_0^2, \end{aligned} \tag{2.20}$$

obtaining finally

$$\omega_0 = \sqrt{\left|\frac{y^{(2)}(t_0)}{y(t_0)}\right| \sin^2\theta(t_0) + \left|\frac{y^{(3)}(t_0)}{y^{(1)}(t_0)}\right| \cos^2\theta(t_0)}. \tag{2.21}$$

2.4 Simulation results of the proposed modeling approach

An almost direct application of the proposed modeling approach leads to a new synchronization algorithm performing tasks comparable to those of a single-phase PLL for grid-connected inverters. As known, a PLL structure must first provide the phase of the grid voltage so as to synchronize the inverter output current with the grid voltage; also using a PLL structure, voltage parameters, such as grid voltage amplitude and angular frequency can be monitored.

In this section five simulation results are reported in order to prove the ability of the proposed method to give fast and accu-

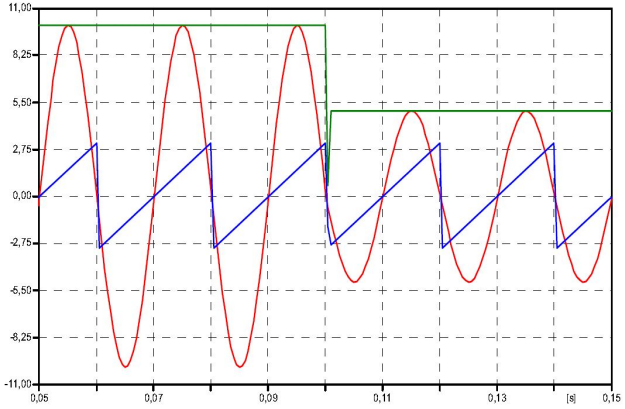

Fig. 2.2. Amplitude and phase-angle estimations in the case of voltage jump

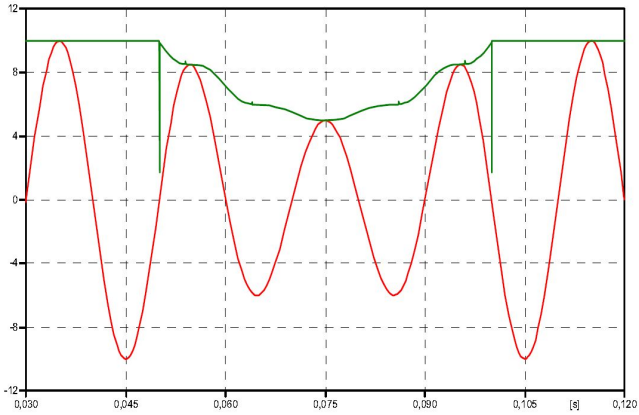

Fig. 2.3. Amplitude estimation during a voltage hole

rate synchronization and reliable monitoring of the amplitude and frequency of the voltage.

In the first case, a sudden jump of the voltage amplitude is considered , whereas the frequency and the phase are constant. Fig. 2.2 shows the corresponding simulation results: the effective voltage signal (in red) characterized only by an amplitude jump at the instant $t = 0.1$s and the estimations of the voltage amplitude (in green) and of the instantaneous phase-angle $\theta(t)$ (in blue). Note as the estimation of the phase-angle is always synchronized with the voltage.

The second simulation experiment refers to a voltage hole of 50% occurring at the instant $t = 0.5$s and which lasts about 50ms. Fig. 2.3 shows the effective voltage (in red) characterized by a maximum decrease of the amplitude equal to 5 Volt and the good tracking of the estimation (in green) of the amplitude obtained by the proposed algorithm.

The third simulation result regards the case of a frequency step from 50 Hz to 51 Hz together a phase variation occurring at

the instant $t = 0.1$s, whereas the amplitude is remained constant. In particular, Fig. 2.4 shows the real frequency (in green) and the estimated value (in red); note how the estimation quickly follows the real value with a very small error.

Fig. 2.5 shows the real voltage waveform (in red) and the estimation of phase-angle $\theta(t)$ (in blue); also in this case, the proposed algorithm allows a fast synchronization with the new phase of the voltage.

In the last simulation experiment a linear frequency variation from 50 Hz up to 60 Hz has been considered. The variation starts at instant $t = 0.05$s and ends at instant $t = 0.1$s, after which the frequency assumes again the value of 50 Hz. Fig. 2.6 shows the effective voltage (in red) characterized by the described frequency variation and constant amplitude and the estimation of phase-angle (in blue). As it can be easily observed, this estimation is always correct and so it is well synchronized with the voltage, regardless of the frequency change.

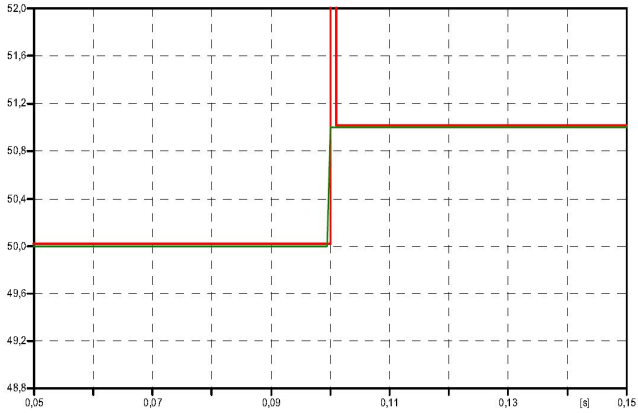

Fig. 2.4. Frequency estimation in the case of frequency jump

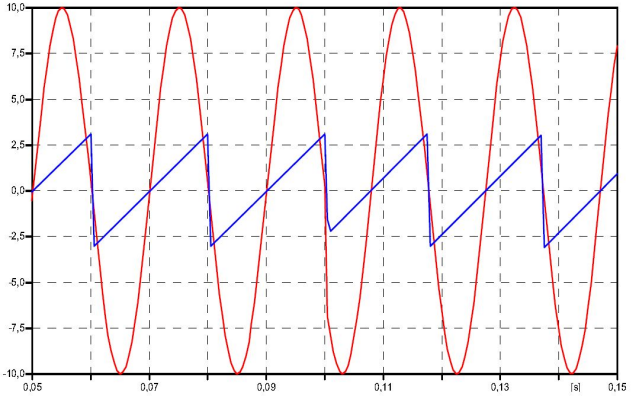

Fig. 2.5. Phase-angle estimation in the case of phase jump

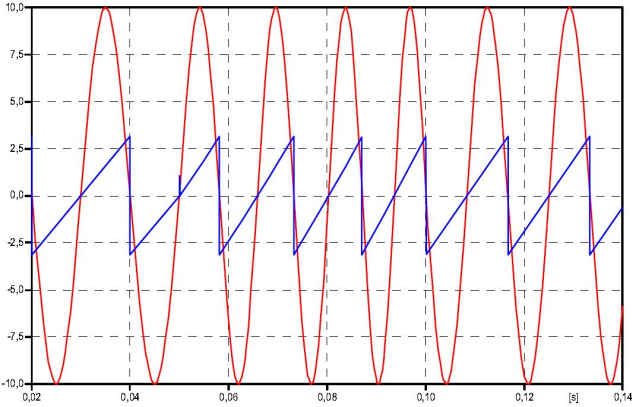

Fig. 2.6. Phase-angle estimation in the case of frequency sweep

2.5 Definition of new instantaneous quantities

As previously said, by the determination of the osculating sinusoid for every instant of time, we can model a signal $y(t)$ as a sinusoidal

signal of amplitude, angular frequency and phase variable at every instant of time and so it can be represented by 2.17.

A significant advantage of this point of view lies in the possibility to define quantities typically considered in sinusoidal steady state conditions also in different situations as during the transients. First of all, it is possible to give new general definitions of active and reactive powers, which can be used in all the situations and are obviously in agreement with those conventional used in the sinusoidal steady-state conditions.

In particular, assuming to modeled the voltage $v(t)$ and the current $i(t)$ according to the proposed approach, i.e as following

$$v(t) = V(t)\sin\theta_v(t) \quad \text{whith} \quad \theta_v(t) = \omega_v(t)t + \varphi_v(t), \tag{2.22}$$

$$i(t) = I(t)\sin\theta_i(t) \quad \text{whith} \quad \theta_i(t) = \omega_i(t)t + \varphi_i(t), \tag{2.23}$$

the instantaneous power can be write as:

$$p(t) = v(t)i(t) = 2P(t)\sin^2\theta_v(t) - Q(t)\sin 2\theta_v(t), \tag{2.24}$$

where $P(t)$ and $Q(t)$ can be defined as instantaneous active and reactive powers respectively and are equal to

$$P(t) = \frac{V(t)I(t)}{2}\cos\left[\theta_v(t) - \theta_i(t)\right], \tag{2.25}$$

$$Q(t) = \frac{V(t)I(t)}{2}\sin\left[\theta_v(t) - \theta_i(t)\right], \tag{2.26}$$

Indeed, in the sinusoidal steady-state conditions i.e. when the voltage and the current are just sinusoidal signals of constant amplitude, phase and frequency, those quantities coincide precisely with the conventional active and reactive powers. As a consequence of the above settings we can also define the quantity:

$$S(t) = \frac{V(t)I(t)}{2} = \sqrt{P^2(t) + Q^2(t)}, \tag{2.27}$$

as instantaneous apparent power and the quantity:

$$\lambda(t) = \cos\left[\theta_v(t) - \theta_i(t)\right] = P(t)/S(t) \tag{2.28}$$

as instantaneous power factor. Similarly, it is possible to extend other definitions usually used in sinusoidal steady-state conditions.

Another interesting result deriving from the proposed approach is connected to the possibility of linking the osculating sinusoid at a certain instant to a phasor representation. In this case, the phasor, usually considered a steady-state concept, may be extended also to the transients because it can be defined as an instantaneous phasor having modulus, frequency and phase variable at every instant of time. Finally, it worthwhile to point that these new definitions, based on the proposed modeling approach, are essentially of single-phase type and therefore they are applicable without major complications to cases in which unbalances and asymmetries in the three-phase systems have to be considered.

2.5.1 Osculating sinusoid approach and p-q Theory comparison

Recalling the description of the *p-q Theory* provided in 2.2, it is easy to understand that the definition provided in (2.28) and (2.26)can be use to analyze the powers flowing through a generic part of the grid instead of the instantaneous powers defined in (2.3). For this reason this section aims present a brief comparison between the instantaneous powers defined by the p-q Theory and those defined by the modeling approach proposed.

In particular, Fig. 2.7 shows the measurements of the instantaneous real power (in green) and the sum of the three instantaneous active powers (in red) absorbed by the load for each phase.

Similarly, Fig. 2.8 presents the instantaneous imaginary power (in green) and the sum of the instantaneous reactive powers (in red).

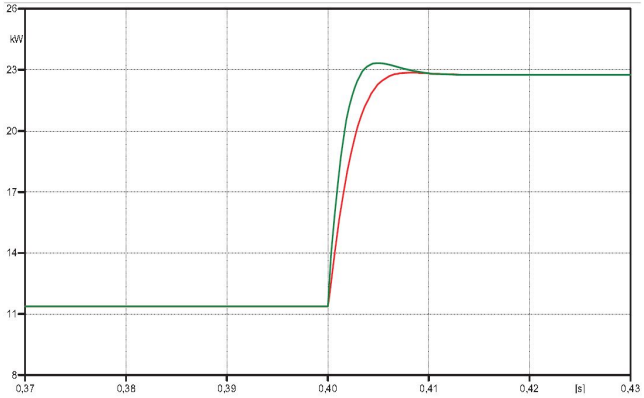

Fig. 2.7. Instantaneous real power and instantaneous active power

As it can be seen, the two approaches provide different values of the instantaneous quantities only during the transient, whereas,

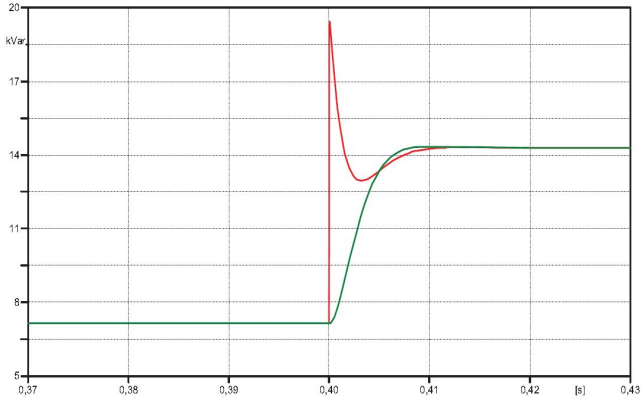

Fig. 2.8. Instantaneous imaginary power and instantaneous reactive power

at steady-state the values of power are the same and, as expected they are in agreement with those conventional used in the sinusoidal steady-state conditions.

2.6 Calculation of the osculating sinusoids parameters for noisy signals

A problem in applying the above modeling approach is due to the fact that the equations used to determine the parameters of the osculating sinusoid, require the knowledge of the signal $y(t)$ and its derivatives up to third order for every instant of time. Indeed, cause the measure of an electrical signal contains at least the acquisition noise,even if suitable numerical differentiation algorithms are adopted, the calculated derivatives, especially those of higher order, are acceptable only for noise-free signals. With the aim to overcome this problem, this section presents new computation techniques which take into account the presence of noise on the signal. Consequently, these techniques, applied to the proposed modeling approach, allows to obtain an algorithm providing a fast and accurate estimation of the frequency, phase and amplitude for noisy signals. The algorithm here presented is divided into three steps, which provide the estimations of the angular frequency, angle phase and amplitude respectively for the osculating sinusoid at the generic instant t_0 . The algorithm is based on the derivatives estimation of noisy signals approaches, recently presented in literature [39],[20] and [51].

2.6.1 Calculation of the osculating sinusoids angular frequency for noisy signals

Let us consider the following expression for the signal

$$r(t) = y(t) + n(t), \tag{2.29}$$

where $n(t)$ is an unstructured perturbation and $y(t)$ is the noise-free signal. To estimate the angular frequency ω_0 of the osculating sinusoid at instant t_0 , we assume to represent the signal $r(t)$ according to the model:

$$r(t) \approx v(t) + n(t), \quad t_0 - T \leq t \leq t_0, \tag{2.30}$$

where $v(t)$ is just the osculating sinusoid at t_0 i.e. $v(t) = V_0 sin(\omega_0 t + \theta_0)$ and T indicates the size of sliding estimation window. This hypothesis can certainly be acceptable, if we use a quite short time window, nevertheless sufficient to obtain accurate estimations. Cause of the use of the Laplace transform in the following analysis we will consider that 2.30 is valid for t¿0.

It is easily to observe that the signal $v(t)$ satisfies the following linear differential equation with constant coefficient:

$$v^{(2)}(t) + \omega_0^2 v(t) = 0, \tag{2.31}$$

Translating this equation into operational domain, we get: ient:

$$s^2 V(s) + 4sv(0) - v^{(1)}(0) + \omega_0^2 V(s) = 0, \tag{2.32}$$

Taking the second derivative with respect to s permits to ignore the initial conditions:

$$2V(s) + 4s\frac{dV(s)}{ds} + (s^2 + \omega_0^2)\frac{d^2V(s)}{ds^2} = 0. \tag{2.33}$$

Then, dividing both sides by s^3 to avoid derivations with respect to time, we have:

$$\frac{2}{s^3}V(s) + \frac{4}{s^2}\frac{dV(s)}{ds} + (\frac{1}{s} + \frac{1}{s^3}\omega_0^2)\frac{d^2V(s)}{ds^2} = 0. \tag{2.34}$$

To estimate the parameter ω_0^2 , it needs to express 2.34 in time domain, using the classic rules of operation calculus. Recalling that the derivation d^k/ds^k with respect to s translates into the multiplication by $(-1)^k t^k$ and $1/s^k$ is replaced by the iterated integral

of order k , we obtain , thanks to Cauchy rule, the estimation of ω_0^2 as the following time-function:

$$\omega_{0e}^2 = -2\frac{\int_0^t \left[(t-\tau)^2 - 4(t-\tau)\tau + \tau^2\right] r(\tau)\, d\tau}{\int_0^t (t-\tau)^2\tau^2 r(\tau)\, d\tau} \tag{2.35}$$

where the noisy observation $r(t)$ is considered in the two integrals. Let us note that (2.35) gives a time domain representation with no derivatives but only integrations with respect to time and the unstructured noise is attenuated by the iterated time integrals, which are simple examples of low pass filters.

Specifying this result to the representation (2.30) and taking into account closely the definition given in the previous section, we obtain for the estimation of the angular frequency $omega_{0e}$ of the osculating sinusoid at instant t_0 , the following formula:

$$\omega_{0e}^2 = 2\left|\frac{\int_0^t \left[(t-\tau)^2 - 4(t-\tau)\tau + \tau^2\right] r(\tau)\, d\tau}{\int_0^t (t-\tau)^2\tau^2 r(\tau)\, d\tau}\right|. \tag{2.36}$$

2.6.2 Calculation of the osculating sinusoids phase-angle for noisy signals

According to (2.7), (2.8) and (2.14), it is easy to obtain the following estimation $\theta_{oe}(t_0)$ of the phase-angle $\theta_o(t_0)$:

$$\theta_e(t_0) = \arctan\left[\omega_{e0}\frac{y_{e0}(t_0)}{y_{e0}^{(1)}(t_0)}\right], \tag{2.37}$$

where $y_{e0}(t_0)$ and $y_{e0}^{(1)}(t_0)$ denote the estimations of the noise-free signal and its first derivative respectively at instant t_0 . Therefore, to obtain the estimation $\theta_{e0}(t_0)$ it is necessary to extract from the samples of the noisy signal $r(t)$ in the interval $[t_0 - T, t_0]$, the estimations of the angular frequency ω_{e0} , the noise-free signal

and its first derivative. The approach, adpoted to calculate these quantities, is based on the assumption that the noise-free signal $y(t)$ can be locally approximated in interval $[t_0 - T, t_0]$ by the truncated Taylor expansion. However, for the sake of simplicity we first consider to represent $y(t)$ in the interval $[0, T]$ by the following polynomial function:

$$y(t) = y(0) + \sum_{h=1}^{N} y^h(0) \frac{t^h}{h!}, \tag{2.38}$$

where N is the approximation degree. In order to obtain a quite accurate estimation of the first derivative of the noise-free signal, a degree N=3 has been chosen in (2.38) i.e. the following expansion has been considered:

$$y(t) = y(0) + y^1(0)t + y^2(0)\frac{t^2}{2} + y^2(0)\frac{t^2}{2} + y^3(0)\frac{t^3}{6}, \tag{2.39}$$

Translating this equation into operational domain, the previous equation is written as:

$$Y(s) = \frac{y(0)}{s} + \frac{y^1(0)}{s^2} + \frac{y^2(0)}{s^3} + \frac{y^3(0)}{s^4}, \tag{2.40}$$

Multiplying both sides of the equality by s^4 and taking the second derivative with respect to s, we have:

$$12s^2Y(s) + 8s^3\frac{dY(s)}{ds} + s^4\frac{d^2Y(s)}{ds^2} = 6sy(0) + 2y^{(1)}(0). \tag{2.41}$$

Dividing by s, taking the derivative with respect to s, again dividing by s^4 and finally using the correspondence rules from operational domain to time domain and the Cauchy rule, the estimation of the first derivative $y_e^{(1)}(0)$ e is given by:

$$y_e^{(1)}(0) = -\frac{60}{T^5}\int_0^T p(\tau)r(\tau)\,d\tau \tag{2.42}$$

with

$$p(\tau) = 2(T-\tau)^3 - 14(T-\tau)^2 + 11(T-\tau)\tau^2 - \tau. \tag{2.43}$$

Because we are interested in obtaining the estimation $y_e^{(1)}(t_0)$, based on the samples of the noisy signal $r(t)$ in the interval $[t_0 - T, t_0]$, it is easy to understand as its formula can be drawn from (2.44) and it has the following expression:

$$y_e^{(1)}(0) = \frac{60}{T^5} \int_0^T p(\tau) r(t_0 - \tau)\, d\tau \tag{2.44}$$

By using an algorithm similar to the previous one, with a degree $N = 2$ in (2.38), the quantity $y_e(t_0)$ is given by:

$$y_e(0) = \frac{60}{T^5} \int_0^T q(\tau) r(t_0 - \tau)\, d\tau \tag{2.45}$$

with

$$q(\tau) = 3(T-\tau)^2 - 6(T-\tau)\tau + \tau^2. \tag{2.46}$$

Once known the estimation $\theta_e(t_0)$, calculated by (2.37), immediately we get the estimation of phase φ_0.

2.6.3 Calculation of the osculating sinusoids amplitude for noisy signals

The estimation of amplitude V_{0e} of the osculating sinusoid at instant t0 is calculated by the equation:

$$V_{e0} = \sqrt{y_e^2(t_0) + \left[y_e^{(1)}(t_0)/\omega_{0e}\right]^2}, \tag{2.47}$$

directly derived by (2.12).

2.7 Numerical experiments

The previous algorithm, applied to the modeling approach of the power electric signals, allows to obtain a method providing a fast and accurate estimation of the frequency, phase and amplitude for noisy grid signals.

In order to explain the performances of this method both during stationary and transient conditions, this section reports some significant numerical experiments. In these experiments, the noise level, introduced in (2.45) and measured by the Signal to Noise Ratio in dB i.e.:

$$SNR = 10 \log_1 0 \left[\frac{\sum y(t_i)^2}{\sum n(t_i)^2} \right], \tag{2.48}$$

has been taken equal to $40dB$; a sliding estimation window $T = 2 \cdot 10^{-3}$s, with 2000 samples has been chosen. Suitable and simple numerical expedients have been used in order to avoid numerical errors in specific conditions. In particular, to avoid zero-crossing of the denominator in (2.36) an appropriate threshold has been adopted.

The first experiment (shown in Fig. 2.9) allows to evaluate the performances of the angular frequency estimation obtained by (2.36). In particular, an abrupt change of the frequency of the signal, from 50 to 51 Hz, has been considered.

Fig. 2.9 shows the frequency variation and the estimation obtained by the method described in section 2.6.1 and already proposed in [39],[20] and [51]. As it is evident, after the step variation, the correct value of the frequency is estimated in less than an half of the signal period.

In order to highlight the performance of the method as regards its ability to provide a good synchronization, the second experiment considers a ramp variation from 50 Hz to 60 Hz for the frequency of the signal.

Fig. 2.10 shows as the estimation of the angle phase $\theta(t)$ is accurate and there is always synchronization between the esti-

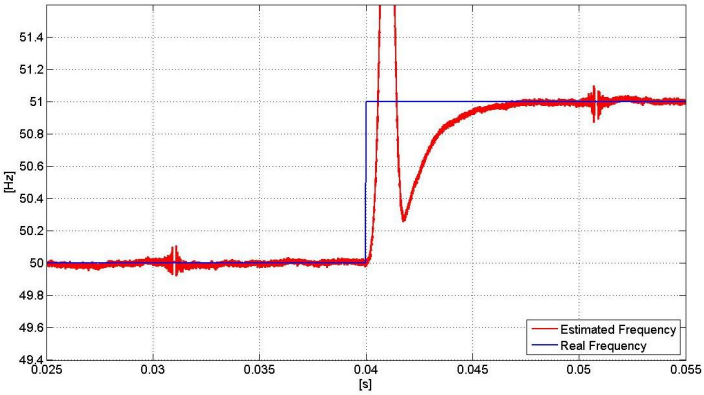

Fig. 2.9. Frequency estimation case of frequency step

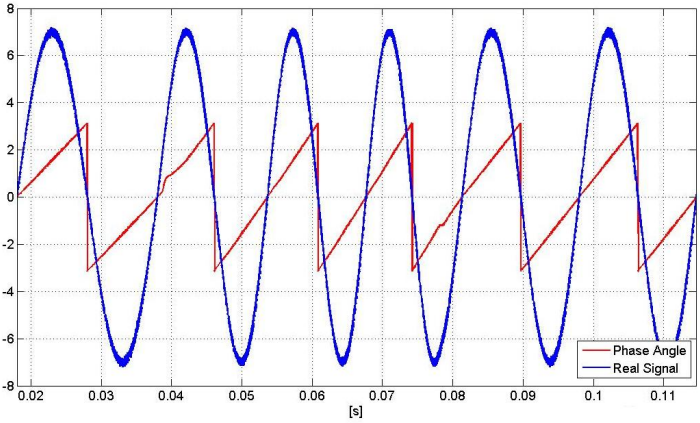

Fig. 2.10. Phase Angle estimation in the case of frequency sweep

mated angle phase and the real signal, also when the frequency is gradually changing.

The third experiment highlights the ability of the proposed method to provide a correct estimation of all the signal parameters. This experiment considers a variation of the signal amplitude which goes from 7 to 5 V and lasts about 90ms.

Fig. 2.11 shows the comparison between real signal and the estimated angle phase and also that between the real signal amplitude variation and its estimation. The figure highlights the good estimation of the signal amplitude obtained also during the transient condition considered, without losing synchronization between the estimation of the angle phase-angle and the real signal.

The last experiment here presented deals with a voltage step of 20% which is the amplitude variation limit defined in UNE-EN 50160 and in UNE-EN 6000-2-4. As it can be seen from Fig. 2.12, the amplitude estimation provided by the proposed method

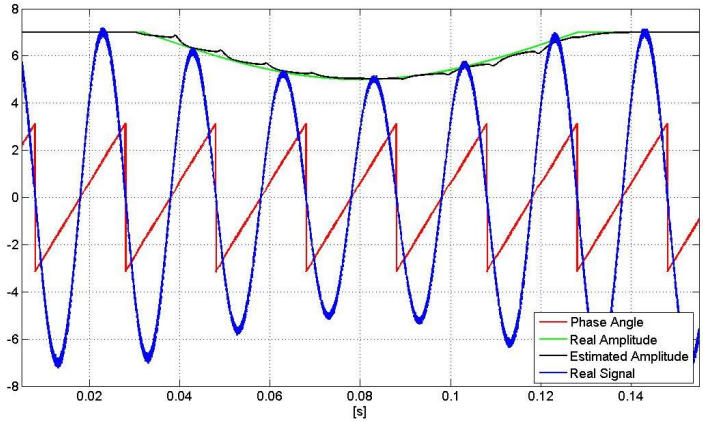

Fig. 2.11. Phase-angle and amplitude estimations in case of voltage hole

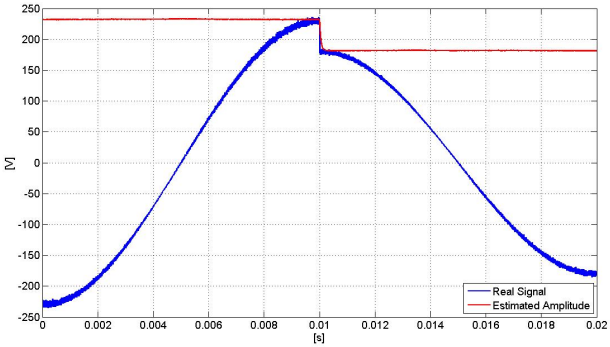

Fig. 2.12. Amplitude estimations in case of voltage step

reaches the reference value with a satisfactory precision and in a very short period.

2.8 conclusion

A new modeling approach for electrical signals in power systems was proposed. The approach is based on the concept, derived from differential geometry, of contact between a signal and an osculating sinusoid at any instant. The method for the calculation of the amplitude, the angular frequency and the phase of the osculating sinusoid was presented.

The effectiveness of the proposed modeling approach was evaluated through different simulation results, regarding its direct application as synchronization algorithm able to give fast and accurate estimations of the amplitude, frequency and phase angle of grid signals.

Moreover, taking into account that the proposed approach allows to model a signal as a sinusoid of amplitude, angular frequency and phase variable over time, new quantities typically considered in sinusoidal steady state conditions but also usable during the transients was defined. In particular, the chapter pointed out as the new definitions of instantaneous active and reactive powers can be seen as an antagonist formulation to the instantaneous power theory, proposed by Akagi et al., and similarly they allow to design control strategies of the power flow in applications based on power electronics converters as DG systems or Power Conditioner equipments connected to the utility grid especially at distribution level.

A difficulty in the application of the proposed approach lies in the calculation of the parameters of the osculating sinusoid (angular frequency, angle phase and amplitude) when the signal contains noise.

Therefore, the chapter dealt with the developed a new computational algorithm for determining the parameters of the osculating sinusoid for noisy signals. This algorithm was obtained by the derivatives estimations of noisy time signals approaches, recently presented in literature. Then, this algorithm, applied to the modeling approach of signals, was used as method providing a fast

and accurate estimation of the frequency, phase and amplitude for noisy grid signals.

3

Power control strategies

This chapter presents a new control strategy for a pulse width modulation (PWM) three-phase voltage source inverter connected to the grid and able to support bi-directional power flow. In particular, the proposed strategy is developed so as to combine the advantages of the Current Control and the Voltage Control. The effectiveness of this combined control strategy is proved by some numerical results compared with those obtained applying only the conventional current control strategy.

Moreover, an application of the proposed control strategy for multibus microgrid is presented.The performance of the proposed application in terms of power management has been verified in simulation on a microgrid test.

3.1 Introduction

The ever increasing energy demand, the necessity of a reduction in costs and higher reliability requirements are driving the present scenario towards Distributed Generation (DG). DG has been considered as a promising alternative for the coordinated and flexible expansion of the present energy distribution system with reduced cost and improved reliability [13]. In particular, small DG systems, typically from 1KW to 10 MW and located near to the loads, are gaining popularity due to their higher operating efficiencies and lower emission levels as provider of electrical energy to the consumers. These DG systems are powered by one or more microsources such as: fuel cells, photovoltaic cells, batteries, windturbine, micro-turbines etc.

Connecting a distributed power system to the electricity grid has potential impacts on the safety and reliability of the grid, which is one of the most significant barriers to the installation of DG technologies. Electric utilities have understandably always placed a high priority on the safety and reliability of their electrical systems. Faced with the interconnection of potentially large number of distributed generators, utilities have perceived DG as a threat. This has led some utilities to place overly conservative restrictions on interconnected systems, causing added costs that may make an installation economically unfeasible. Several techniques may reduce adverse network impacts allowing DG connection, but those techniques can be project specific and may be expensive, and adversely affect project economics [5].

To reduce the impact in the power grid several requirements are needed. Typically, equipment that prevents power from being fed to the grid when the grid is de-energized,are included; moreover,*power quality* features are required such as limits on the interconnected systems effects on flicker, harmonic distortion, and other types of waveform disturbance. Systems may also be required to automatically shut down in the event of electrical failures, to provide an isolation transformer for the system, as well as to provide liability insurance.

The electric power system interface is the means by which the DG unit electrically connects to the power system outside the facility in which the unit is installed. In simple terms, "interconnected with the grid" means that both the DG system and the grid supply power to the facility at the same time. Paralleled systems offer added reliability, because when the DG system is down for maintenance, the grid meets the full electrical load, and vice versa. Distributed generation systems can be designed to keep a facility up and running without an interruption if the grid experiences an outage. Also, grid-interconnected systems can be sized smaller to meet the customers base load as opposed to its peak load. Not only is the smaller base-load system cheaper, it also runs closer to its rated capacity and, therefore, is more fuel efficient and cost-effective.

As example, it is usual practice to connect PV systems to the local electricity network. This means that, during the day, the electricity generated by the PV system can either be used immediately (which is normal for systems installed in offices, other commercial buildings, and industrial applications) or be sold to one of the electricity supply companies (which is more common for domestic systems, where the occupier may be out during the day). In the evening, when the solar system is unable to provide the electricity required, power can be bought back from the network. In effect, the grid is acting as an energy storage system, which means the PV system does not need to include battery storage [22].

Moreover, many microsources generate electric power in a waveform that the present power distribution grid cannot accept. Photovolatic cells or fuel cells supply DC electric energy while the present distribution grid accepts AC electric energy, therefore specific converters are necessary for the DC to AC conversion.

Furthermore, in some cases wind power generation systems use a controlled rectifier to convert the AC voltage from wind turbine generator to DC voltage, being the frequency and amplitude of the AC voltage from the wind turbine generators variable in time due

to the random nature of the wind; so also in this case, a converter is required.

The above characteristics can be obtained thanks to the use of grid-connected inverters able to quickly manage power generated by the microsources and to generate reactive power near loads, allowing losses reduction.

Recently, increased research efforts have been focused on both the control and the topologies of the grid-connected inverters [52],[44],[48]. The desirable features for these inverters are low line current distortion and high power factor, high efficiency, high switching frequency and simply circuitry.

The aim of this chapter is to discuss control strategies for a pulse width modulation (PWM) three and single phase voltage source inverter (VSI) able to support bidirectional power flow and so to be operate as interface between a DC power source and the AC distribution grid.

In the following it will be supposed that the DC source are supplied from AC generator (by AC-DC converter), or DC power source (by DC-DC converters). Moreover, the presence of storage devices such as batteries used as buffers to provide short-term transient high power requirements will be taken into account; just in this case, it is important that the grid-connected inverter is able to support bi-directional power flow that is it operates also as rectifier to draw power from the AC distribution grid to charge the batteries.

Starting from the consideration that an inverter working with reverse power flow controlling the DC voltage is a PWM regenerative rectifier, a new control strategy developed so as to combine the advantages of the Current-Controlled PWM Rectifier and the Voltage-Controlled PWM Rectifier [19] will be presented. As it known, the former strategy should be preferred to ensure stability of the whole conversion system, while the latter one allows a more accurate generation of the reference voltages necessary to apply the PWM voltage technique.

3.2 The Grid-connected Inverter

With the development of solid-state-based packages, power electronic devices can now convert almost any form of electrical energy to a more desirable and usable form. This is why power electronic interfaces are ideal for DG system applications.

As already explained, many power sources used in DG systems generate electric power in a waveform that the present power distribution grid cannot accept. Sources as photovoltaic cells or fuel cells supply dc electric energy, while the present distribution grid accepts ac electric energy. More often, in the near future, wind power generation systems will need to convert the ac voltage from wind turbine generator to dc voltage, being the frequency and amplitude of the ac voltage from the wind turbine generators variable in time due to the random nature of the wind. As a consequence, the power electronic interfaces may include both ac-dc conversion systems (rectifiers) and dc-ac conversion systems (inverters).

Another benefit of power electronic devices is their extremely fast response times; in fact, the dc-ac power interface, usually called grid-connected inverter, can respond to power quality events or fault conditions that occur in the grid within the sub-cycle range.

In addition to allowing the transfer of power supplied by the microsource of the DG system, the grid-connected inverter can also permit the control of voltage and reactive power at the PCC of the generation source [2]. In particular, most inverters for DG systems are self commutated and can produce an ac voltage of an arbitrary amplitude and phase. This allows the DG systems to produce any power at any power factor so as a wider operating power factor range than a synchronous generator can be obtained.

The grid-connected inverter can also contain protective functions, for both the distributed energy system and the local electric power system, that allow paralleling and disconnection from the electric power system. Moreover, also some level of metering and control functionality are contained and this shall ensure that the distributed energy system can operate as designed.

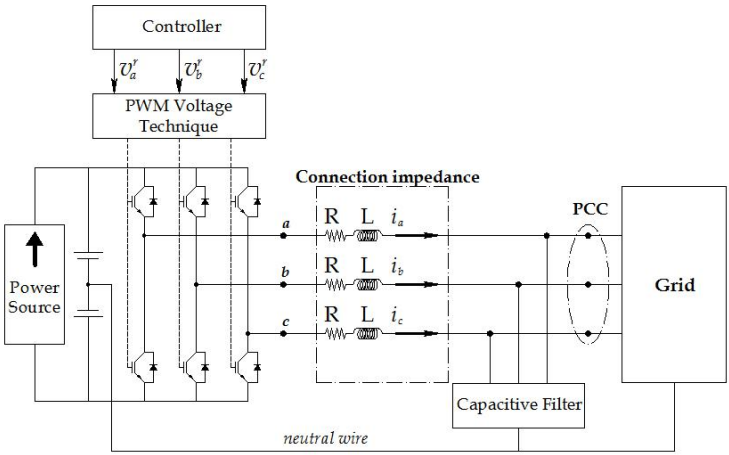

Fig. 3.1. Grid-connected inverter configuration.

Finally, it is worth to highlight that the grid-connected inverter controls must ensure different important requirements: new microsources can be added to the system without modification of existing equipment, set-up can be independently chosen, shares of grids can connect to or isolate itself from the main-grid in a rapid and seamless fashion, reactive and active powers can be independently controlled and can meet the dynamic needs of the loads.

The configuration of the grid-connected inverter, considered, is reported in Fig. 3.1. It comprises a three-leg VSI connected on the ac-side to the grid by a suitable connection impedance and on the dc-side to a dc-power source by capacitors. The inverter works in order to transfer the energy produced by the dc-power source on the grid, controlling the power flows through the connection impedance. This is constituted by three connection impedances each with resistance R and inductance L and a parallel capaci-

tive filter providing a path for some high-order harmonics at the switching frequency.

Considering that the inverter operates in voltage control mode, its controller generates three reference signals v_j^r (where $j = a, b, c$), each of which is referred to the output voltage to be applied on the $j-th$ phase, so that the connection impedance current i_j tracks its desired value corresponding to the power flows required between the DC and AC sides. Obviously, it is needed that the output voltages of the VSI v_j ($j = a, b, c$) track the reference voltages by properly applying the PWM technique; so in the following it will be assumed that $v_j^r = v_j$.

3.3 Power flow control analysis

The equations which rules the power flow control can be obtained by considering the simple circuit of Fig. 3.2. It shows the voltages and the currents relevant to the branch $\boldsymbol{a}$ of the connection impedance.

The basic idea of the power flow control consists in the control of the current through the connection impedance. As easy to see, the VSI can effect the current control by imposing the voltages produced and then the voltage drop on the connection impedance. Under sinusoidal stationary condition quite simple analysis can be carried out to determine the correct value of voltages that has to be generate by the inverter: bond between the circuit voltages and current can be analyzed by means of classical phasor diagram. Obviously, under not sinusoidal and especially transient condition the use of phasor diagram become impossible so that almost all power control strategies recently proposed consider the use of direct current control algorithms.

As already explained the possibility to deal with transient phenomenon is an important issue in the application field we are considering. For this reason, in the following all voltages and currents have to be considered time dependent with generic waveform, as

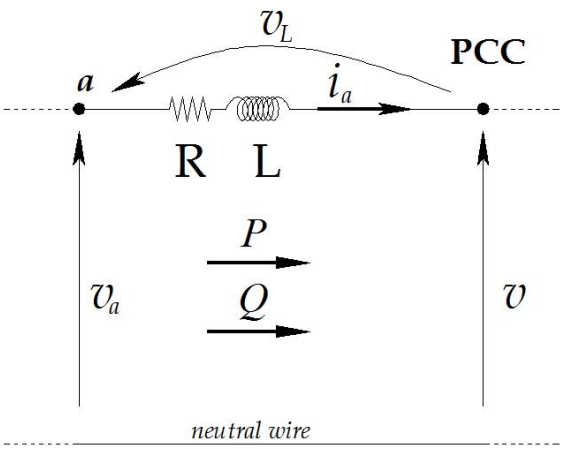

Fig. 3.2. Connection impedance circuit.

well as $\boldsymbol{P}$ and $\boldsymbol{Q}$ which should at lest track the variation of the conventional active an reactive power respectively.

Fig. 3.3 shows a block diagram of a conventional control current of a grid-connected inverter relative to one generic phase (where the subscript j is omitted). The block A, operating as phase locked loop, provide the estimation the rms value V and the phase-angle θ_v of the PCC voltage v.

In Fig. 3.3, P^* and Q^* represent the desired values for the active and reactive power respectively. Their choice is independent on the Current Control strategy and can be effected in different ways: Q^* can be chosen equal to the reactive power absorbed by the load in order to realize the load power factor correction or it is set equal to zero so as to assure a connection of the renewable generation system to the AC grid distribution with a unitary power factor. P^* can be obtained in order to achieve the desired voltage value of the DC bus or also to balance a unbalanced load.

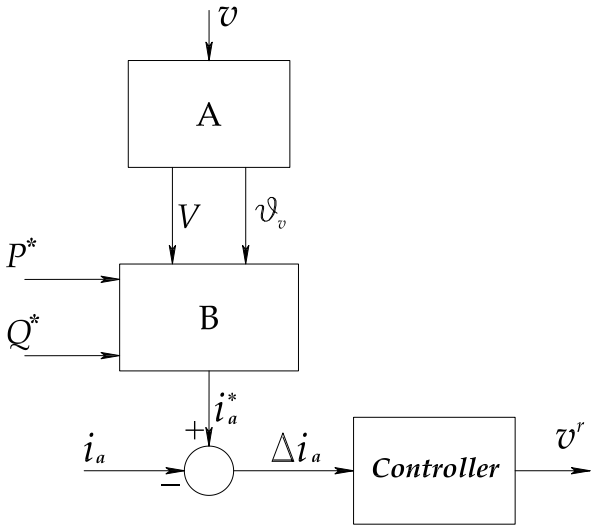

Fig. 3.3. Current control diagram block.

The block B uses the values V and θ_v to calculate the instantaneous value of the reference current i_a^* necessary to obtain the desired power flows.

Then, on the basis of the difference between the reference current and the actual current i_a, a suitable regulator (*controller*) determines the reference voltage signal v^r.

In this kind of control the two most important issues are the choice of the block A and of the current *controller*. It is important to say that usually, the choice of the two block laws is carried out totally independent each other, even if their operation is strictly dependent. In particular, the choice of the controller law can be effected in different ways: hysteresis or delta controller, PI regu-

lator, predictive controller and resonant controller. Hysteresis or delta controllers assure an effective track of the reference voltage value with low requirement in terms of computational burdens. However the high frequency switching needed by this kind of controller brings poor performance in terms of efficiency. PI controller is one of the most used solution especially in three phase control scheme, where a rotating frame of reference signal can be used. In a single-phase scheme like that shown in Fig. 3.3 PI controllers have the shortcoming to present a phase error during steady-state operating and a limited ability to reject disturbance. The phase error result in a power factor decrement and the limited disturbance rejection capability leads to the need of a feed-forward compensation. However the imperfect compensation action of the feed-forward control due to background distortions result in high harmonic distortion of the current.

The predictive controllers are based on the common principle to foresee the evolution of the controlled variable so as to choose the state of the converter or the average voltage produced by the converter. Among these controllers the dead-beat regulator is based on the estimation of the derivative of the variable to control so as to predict the effect of the control action. The controller is developed on the basis of the model of the filter and of the grid, so it is sensitive to model and parameter mismatches.

The resonant controllers are based on the use of Generalized Integrator. Thanks to the use of a double integrator, they presents an infinite gain at a resonance frequency and almost no attenuation outside this frequency. Using this kind of controller it is possible to reduce phase error during stationary conditions and perform selective disturbance rejection compared with PI controller. However, it has to be considered that the tuning of the resonant frequency involves the a-priori knowledge of the control signal frequency.

3.4 A new power flow control strategies

This section presents a new control strategy which, making use of the modeling approach described in Chap. 2, combines voltage control and current control so as to obtain a synergic action in the power flow management. A preliminary part of this section deals with some important new concepts which will be used to develop the proposed control strategy. In particular, considering as example the case of a inductive circuit, it will be explain how to link the circuit currents and voltages according to the modeling approach, so as to show an original way to analyze circuit waveform during transients. It is important to make precise that all the results are not in disagreement with the classical laws which describe transients in electric circuit, being only a different point of view to study transient phenomena.

The following two parts of this section will explain in detail the voltage control and the current control used together in the proposed control approach. In the final subsection the control scheme of the proposed control strategy will be illustrated

3.4.1 Instantaneous circuit analysis

As already said, the basic idea of the power flow control consist in the control of the current through the connection impedance shown in Fig. 3.2. As known the bond between the current flowing through the connection impedance and the voltage v_L is expressed by the following differential equation

$$\frac{di_a}{dt} = -\frac{R}{L} i_a + \frac{1}{L} v_L, \tag{3.1}$$

which, as known, has the following solution

$$i_a = e^{-\frac{R}{L}t} \left(\int \frac{1}{L} v_L(\tau) e^{\frac{R}{L}\tau} d\tau + C \right), \tag{3.2}$$

where, obviously, C is the constant depending of the starting conditions. Assuming to model v_L, at the instant t_0, according to the modeling approach described in 2.3, it is possible to approximate, for the short interval $[t_0 - dt, t_0]$ the voltage v_L by its osculating sinusoid, i.e.

$$v_L(t) \approx V_0 \sin(\omega_0 t + \varphi_0), \quad t_0 - dt < t < t_0, \tag{3.3}$$

where V_0, ω_0 and φ_0 are the amplitude, the angular frequency and the phase of the osculating sinusoid of v_L at the instant t_0.

Then, considering (3.3) it is possible to approximate the value of the current i_a at the instant t_0, by the following relation

$$i_a(t_0) \approx \bar{i}_a(t_0) e^{-\frac{R}{L}dt} + \widetilde{i}_a(t_0) \tag{3.4}$$

where clearly is

$$\bar{i}_a(t_0) = \left\{ i_{a0} - \frac{V_0}{\sqrt{R^2 + L^2\omega_0^2}} \sin\left[\omega_0(t_0 - dt) + \varphi_0 - \arctan\left(\frac{L\omega_0}{R}\right)\right] \right\} \tag{3.5}$$

and

$$\widetilde{i}_a(t_0) = \frac{V_0}{\sqrt{R^2 + L^2\omega_0^2}} \sin\left[\omega_0 t_0 + \varphi_0 - \arctan\left(\frac{L\omega_0}{R}\right)\right] \tag{3.6}$$

with $i_{a0} = i_a(t_0 - dt)$.

Then, according with the modeling approach of Chap. 2, it is possible to define $Z_0 = \sqrt{R^2 + L^2\omega_0^2}$ and $\rho_0 = \arctan(L\omega_0/R)$ as the instantaneous magnitude and phase of the connection impedance of Fig. 3.2. It is then possible rewrite (3.6) as

$$\widetilde{i}_a(t_0) = \frac{V_0}{Z_0} \sin(\omega_0 t_0 + \varphi_0 - \rho_0) \tag{3.7}$$

As easy to see, using the proposed modeling approach, it has been possible to isolate a share of the connection impedance current which can be tied to representation of the voltage v_L in a

similar way compared to the rules conventionally used in sinusoidal steady-state condition. In fact, so as explained in 2.5, being the instantaneous phasor of $v_L = V_0 \sin\theta_0$ (with $\theta_0 = \omega_0 t_0 + \varphi_0$), at the instant t_0, equal to $V_0 e^{j\theta_0}$, we can express $\widetilde{i}_a$ in terms of instantaneous phasor as $V_0/Z_0 e^{j\left(\theta_0 - \frac{\pi}{2} - \rho\right)}$. However, this proves that controlling the voltage across the connection impedance by using the concept of instantaneous phasor, we can control only a share the desired current. Then, from this point of view, the portion of current $\bar{i}_a$ have to be considered an undesired quantity, which should be suppressed in order to obtain the desired current flow.

Let us note from (3.5) and (3.6) that being $t_0 - dt \approx t_0$ and $e^{-\frac{R}{L}dt} \approx 1$, then $\bar{i}_a$ can be approximate as

$$\bar{i}_a(t_0) \approx i_{a0} - \widetilde{i}_a(t_0). \tag{3.8}$$

This means that to suppress $\bar{i}_a$ we will have to force the current to its desired value. From this result can be figured out why the knowledge of the actual current value is needed to perform the correct power exchange during transients.

3.4.2 Voltage control strategy

For sake of simplicity only the powers exchange on the phase "***a***" of the circuit of Fig. 3.1 will be analyzed, because the relationships that rule the power flows through the others phases can be obtained in a similar way. Moreover, in this subsection only the current component $\widetilde{i}_a$ will be considered, being the control of the component $\bar{i}_a$ analyzed in the next subsection.

On the basis of the analysis carried out until now, by expressing the voltage at the PCC node $v(t)$, the output voltage produced by the inverter $v_a(t)$, the current component $\widetilde{i}_a(t)$ and the voltage across the connection impedance $v_L(t)$ by their instantaneous phasors $\mathbf{V}(t)$, $\mathbf{V}_a(t)$, $\widetilde{\mathbf{I}}_a(t)$ and $\mathbf{V}_L(t)$ respectively and choosing $\mathbf{V}(t)$ as the reference one, the instantaneous phasor diagram shown in Fig. 3.4 is obtained.

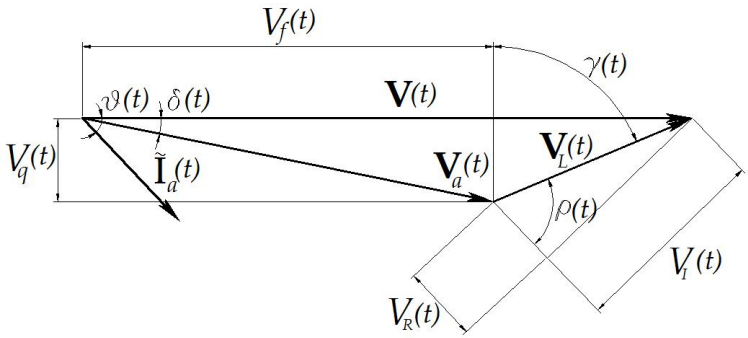

Fig. 3.4. The instantaneous phasor diagram relevant to the circuit of Fig. 3.2.

Obviously, the diagram of Fig. 3.4 is related to a particular instant t and then all the quantities represented have to be considered time dependent with generic waveform. In detail: $\delta(t)$ is the phase angle of $\mathbf{V}_a(t)$, $V_f(t)$ and $V_q(t)$ can be defined as the forward and the quadrature components of $\mathbf{V}_a(t)$ with respect to $\mathbf{V}(t)$; $\theta(t)$ is the phase angle of $\widetilde{\mathbf{I}}_a(t)$; $\rho(t)$ is the characteristic angle of the connection impedance; the angle $\gamma(t)$ is defined by the following relationship

$$\gamma(t) = \frac{\pi}{2} + \theta(t) - \rho(t). \tag{3.9}$$

Moreover, the magnitude of the resistive and the inductive voltage components of $\mathbf{V}_L(t)$, $V_R(t)$ and $V_I(t)$ respectively, are obviously defined as

$$V_R(t) = V_L \cos\rho(t) \quad V_I(t) = V_L \sin\rho(t), \tag{3.10}$$

where $V_L(t)$ is the amplitude of $\mathbf{V}_L(t)$.

As explained in 2.5, we can define the active and reactive instantaneous power flows from the node "$\boldsymbol{a}$" to the PCC by the following relationships

$$P(t) = \frac{V(t)\widetilde{I}_a(t)}{2}\cos\theta(t) \quad Q(t) = \frac{V(t)\widetilde{I}_a(t)}{2}\sin\theta(t). \tag{3.11}$$

Considering (3.11) and the amplitude of the connection impedance current, it is possible to obtain the following law for the instantaneous active and reactive powers

$$P(t) = \frac{V(t)}{2Z(t)}\frac{V_I(t)}{\sin\rho(t)}\cos\theta(t) \quad Q(t) = \frac{V(t)}{2Z(t)}\frac{V_I(t)}{\sin\rho(t)}\sin\theta(t) \tag{3.12}$$

where $Z(t)$ is the instantaneous amplitude of the connection impedance.

From the phasor diagram of Fig. 3.4, it is easy to observe that

$$V_I(t)\cos\theta(t) = V_a(t)\sin\rho(t)V_R(t)\sin\theta(t) \tag{3.13}$$

$$V_L(t)\sin(\rho(t)-\theta(t)) = V_a(t)\sin\delta(t) = V_q(t) \tag{3.14}$$

Then, considering the first one of (3.10) and using the Werner formulas, it is possible rewrite

$$P(t) = \frac{V(t)}{2Z(t)}\frac{V_I(t)+V_L\sin(\theta(t)+\rho(t))}{2\sin\rho(t)}. \tag{3.15}$$

Moreover, from the phasor diagram of Fig. 3.4, the following angular relationship can be easily obtained

$$\theta(t)+\rho(t) = \gamma(t)-(\pi/2-\rho(t)). \tag{3.16}$$

therefore, by means simple algebraic manipulation, it can be obtain

$$\sin(\theta(t)+\rho(t)) = 2\sin\gamma(t)\sin\rho(t)\cos\rho(t) - \left(\cos^2\rho(t)-\sin^2\rho(t)\right)\cos\gamma(t). \tag{3.17}$$

Consequently, by substituting (3.17) in (3.15) and observing, from Fig. 3.4, that

$$P(t) = \frac{V(t)}{2Z(t)} \left[\sin \rho(t) V_q(t) + cos\rho(t) \left(V(t) - V_f(t)\right)\right]. \quad (3.18)$$

In a similar way it is possible to provide the relationship which describe the bond between the voltages on the connection impedance and the instantaneous reactive power flows supplied by the inverter:

$$Q(t) = \frac{V(t)}{2Z(t)} \left[\sin \rho(t) \left(V(t) - V_f(t)\right) - cos\rho(t) V_q(t)\right]. \quad (3.19)$$

Neglecting the resistance of the connection impedance, i.e. considering $\rho = \pi/2$, the expressions for the instantaneous active and reactive power flows become

$$P(t) = \frac{V(t)}{2X(t)} V_q(t), \quad Q(t) = \frac{V(t)}{2X(t)} \left(V(t) - V_f(t)\right), \quad (3.20)$$

where $X_L(t)$ is the instantaneous amplitude of the connection reactance.

These equations show that, for purely inductive connection impedance, the instantaneous active power flow only depends on $V_q(t)$, while the reactive power flow only depends on $V_f(t)$; therefore, by controlling the forward and the quadrature component of $\mathbf{V}_a(t)$ (i.e. the amplitude and the phase angle of $\mathbf{V}_a(t)$ with respect to $\mathbf{V}(t)$), it is possible to control the instantaneous active and reactive power flows of the circuit of Fig. 3.2.

It is worth to underline that in the real case the resistance R is not just equal to zero, but surely it is very low, representing a parasitic resistance of an inductive filter; therefore (3.20) can be considered as acceptable approximations of (3.18) and (3.19).

3.4.3 Current control strategy

The voltage control presented can be considered as an indirect control of the connection impedance current. However, as already explained, the voltage control allows to control only a share of the connection impedance current. Then, a direct control of the current is necessary so to allow the correct power exchanges.

Due to the presence of the inductance L in the circuit of Fig. 3.2 the amount of energy needed to cancel $\bar{i}_a$ can be expressed as

$$E = \frac{1}{2} L \left(i_{a0} - \widetilde{i}_a \right)^2 . \tag{3.21}$$

Then, on the basis of the analysis carried out until now, the more appropriate action to suppress $\bar{i}_a$ is to apply voltage corrective component proportional to the energy needed to take the actual value of the current i_{0a} to its desired value $\widetilde{i}_a$.

3.4.4 Power flow control algorithm

The block diagram relevant to the control strategy applied to the phase $\boldsymbol{a}$ of the grid-connected inverter, is shown in Fig. 3.5 (where for sake of simplicity the argument t of the variables is omitted).

As clearly evidenced, the two control parts are indicated with Voltage Control and Current Control respectively. Both the parts need the estimation value for the instantaneous amplitude V and the phase-angle θ_v of the correspondent PCC voltage v (obtained by block A operating according to the modeling approach described in 2.3.1) and information about the desired power flows P^* and Q^* to be exchanged with the grid. Then, the reference voltage v^r is obtained as sum of two contributions: v_v^r given by the Voltage Control and v_c^r given by the Current Control.

The *Voltage Control* marked in Fig. 3.5 is simply realized through the two blocks C and D. In fact, on the assumption that the connection filter is purely inductive, the block C calculates V_q and V_f according to the following equations, directly obtained from (3.20)

$$V_q(t) = 2P^*(t)\frac{X(t)}{V(t)}, \quad V_f(t) = V(t) + \frac{X(t)}{V(t)}2Q^*(t), \tag{3.22}$$

and block D determines the share $v_v^r(t)$ of the reference voltage on the basis of the following relationships

$$v_v^r(t) = \sqrt{V_q^2(t) + V_f^2(t)}\sin\left(\theta_v(t) + \delta(t)\right), \tag{3.23}$$

where

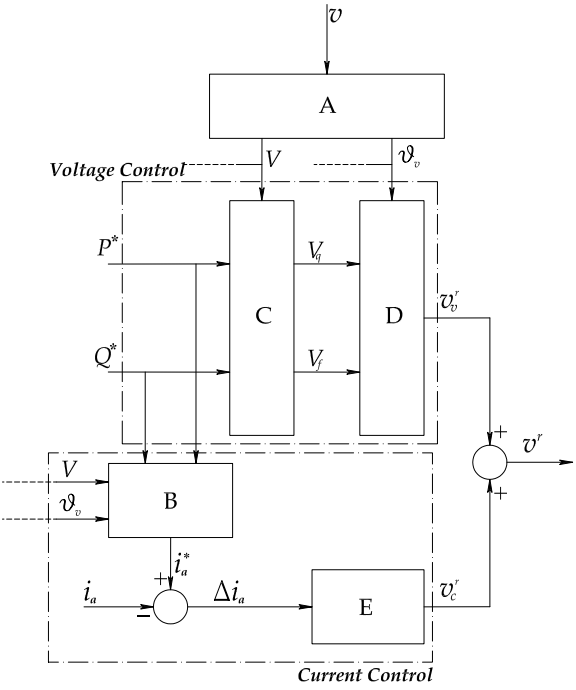

Fig. 3.5. Block diagram of the combined control strategy.

$$\delta(t) = \arctan\left(\frac{V_q(t)}{V_f(t)}\right). \tag{3.24}$$

The block B, included in the *Current Control*, uses V and θ_v to calculate the instantaneous value of a reference current i_a^* necessary to obtain the desired power flows $P^*(t)$ and $Q^*(t)$, by means of the following equation

$$i_a^*(t) = \widetilde{I}_a^*(t)\sin\left(\theta_v(t) - \varphi_i(t)\right), \tag{3.25}$$

where

$$\varphi_i(t) = \arctan\left(\frac{Q^*(t)}{P^*(t)}\right), \quad \widetilde{I}_a^*(t) = \frac{\sqrt{\left(P^*(t)\right)^2 + \left(Q^*(t)\right)^2}}{V(t)} \tag{3.26}$$

The block E represents the regulator determining, on the basis of the error $\Delta i_a(t) = i_a^*(t) - i_a(t)$, the other share $v_c^r(t)$ of the reference voltage. As already said, the amount of energy needed to take the actual value of the connection impedance current to its desired value is given by (3.21). Then, the control law for the block E has been choose equal to:

$$v_c^r(t) = k\Delta i_a^2(t)\texttt{sign}\Delta i_a(t), \tag{3.27}$$

represented by the instantaneous characteristics shown in Fig. 3.6 and where k is a suitable constant.

3.5 Numerical results

The achievement of a right synergy of the voltage and current control actions given by the proposed control strategy is demonstrated by the numerical simulations shown in Fig. 3.7 and Fig. 3.8. The former figure reports the voltage reference v_v^r and v v_c^r , obtained by the Voltage and Current Control respectively, and the

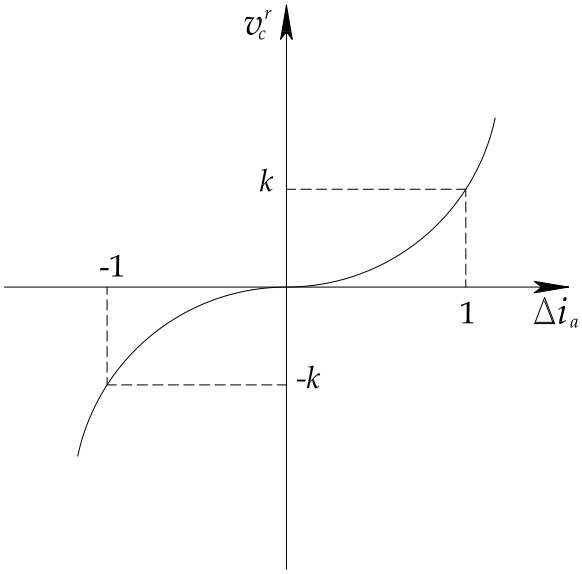

Fig. 3.6. Instantaneous characteristics of the *Current Control* regulator (block E).

total voltage reference v^r; the second figure shows the comparison between the reference current i_a^* and the actual current i_a.

From these results it is easy to observe that a valuable action of the current control is carried out just only during a short transient and it finishes when the value of the current generated by the inverter has substantially reached the desired value; then, the support of the current control part is practically equal to zero during steady-state condition.

The results of Fig. 3.9 and Fig. 3.10 have the purpose to highlight a comparison on the performances of the conventional *Current Control*,which use a PI regulator for current control, and the combined *Voltage and Current Control*. In particular, both fig-

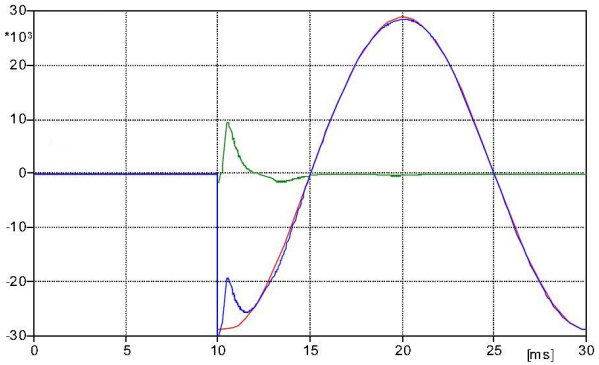

Fig. 3.7. Voltage references for the proposed control strategy.

ures show the behaviors of the reference current i_a^* (in green) and the actual current i_a (in red), when a sudden variation of the desired values of the power flows P^* and Q^* occurs, starting from a generic time instant.

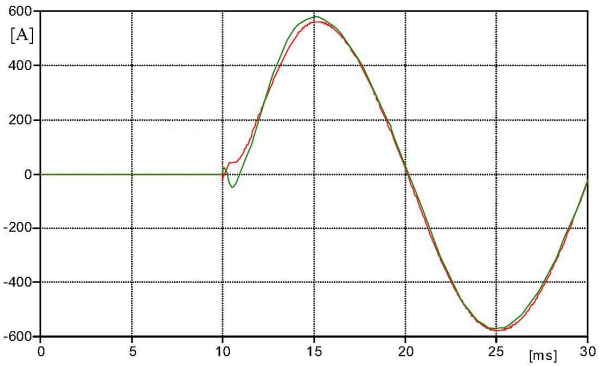

Fig. 3.8. Comparison between the actual current (in red) and reference current (in green).

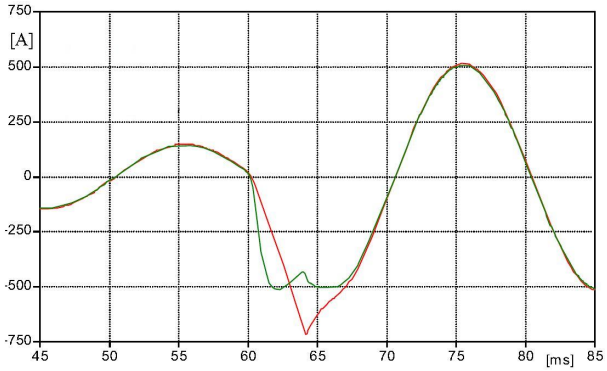

Fig. 3.9. Behaviors of the actual current (in red) and reference current (in green) for the conventional *Current Control*.

The comparison of the two figures evidences clearly the proposed control strategy enables a tracking of the reference current during the transient period much more acceptable than that corresponding to the Conventional Current Control.

Moreover, it has been observed that, as many experiments suggest, the choice of the gain k of the current regulator E for the proposed combined control strategy can be effected in a wide range of values avoiding instability problems. In fact, different values of that parameter simply involve or a small delay in the current tracking or a light harmonic content in the reference voltage.

On the contrary, as previously said, the choice of the gains of the regulator PI for the Conventional Current Control involves some difficulties. For example, an improvement of the transient behavior can be obtained to expenses of results about the steady-state performance.

Another interesting comparison between the two strategies of control is obtained by the examination of the waveforms of the reference voltages. For this purpose, Fig. 3.11 and Fig. 3.12 report the signal reference voltage v^r obtained by the conventional

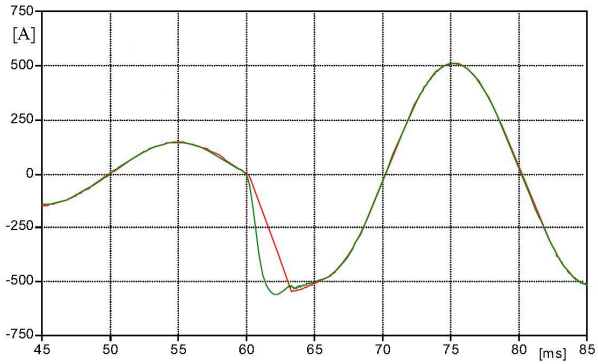

Fig. 3.10. Behaviors of the actual current (in red) and reference current (in green) for the combined *Voltage and Current Control*.

Current Control and the combined *Voltage and Current Control* respectively. It is evident that the reference voltage of Fig. 3.12 and corresponding to the proposed control strategy has a significantly reduced harmonic content.

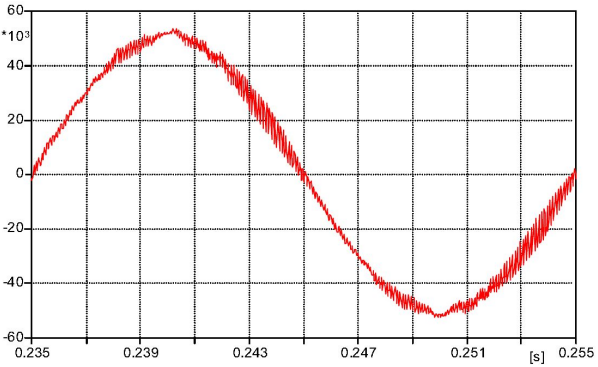

Fig. 3.11. Voltage reference for the conventional *Current Control*.

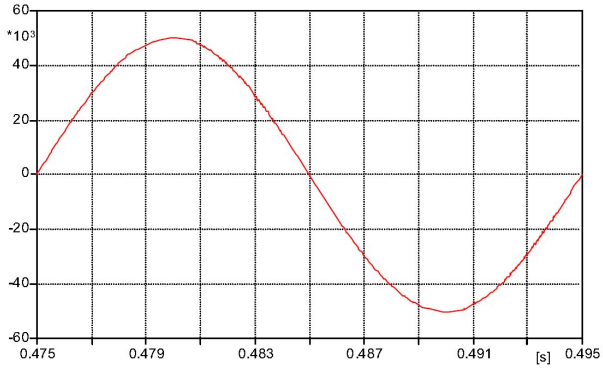

Fig. 3.12. Voltage reference for the combined *Voltage and Current Control*.

3.6 Microgrid application of the combined Voltage and Current control

A recent evolution resulting by the diffusion of the DG systems is emerged with the concept of Microgrid, which consists in a cluster of loads and paralleled DG systems operating as a single power system that provides power to its local area [28]. A Microgrid is a systematic organization of DG systems and therefore it has larger capacity and more control flexibility to fulfill system reliability and power quality requirements, in addition to all the inherent advantages of a single DG system.

As evidenced by the argumentation exposed in the previous sections, the above characteristics can be obtained thanks to the use of grid-connected inverters used to manage the power generated by the microsources and to generate reactive power near loads so as allow losses reduction. In this specific case, it is important that the grid-connected inverters operates without communication links with the paralleled DG systems, which can be located far apart; thus, the control algorithms of each individual

DG system should be based on feedback variables that can be measured locally and moreover, they have to ensure a safety operation of the Microgrid avoiding instability problems, which can occur especially when many DG systems are located in a same area.

A good solution for the aforementioned problems can be obtained by the application proposed in the following. It is based on the use of a control strategy for grid-connected inverters able to dynamically change the energetic contribution of the microsources, that so adapts oneself to variations of the grid characteristics and contributes to the power management of the Microgrid.

The performance of the proposed application is verified in simulation on a Microgrid test, in which several DG systems are contemporary connected to the main bus.

3.7 Microgrid concept

It is a widespread opinion that small generation should be part of the building energy management systems. In all likelihood, the DG energy output would be ran more cost-effectively with a full range of energy resource optimizing: peak-shaving, power and waste heat management, centralized load management, price sensitive fuel selection, compliance with interface contractual terms, emissions monitoring/control and building system controls. The Microgrid paradigm provides a general platform to approach power management issues.

It has been found that, in terms of energy source security, multiple small generators are more efficient than relying on a single large one for lowering electric bills [43]. Small generators are better at automatic load following and help to avoid large standby charges seen by sites using a single generator. Having multiple DG systems on a Microgrid makes the chance of all-out failure much less likely, particularly if extra generation is available.

Moreover, as already explained, the DG systems in Microgrid are generally powered by emerging technologies such as photovoltaic or wind-power and often equipped by inverters to interface with the electrical distribution system. The major issue with these technologies is the nature of the generation; indeed, the availability of their energy source is driven by weather and not by the loads of the systems. These technologies can be labelled as intermittent and ideally they should be operated at maximum output.

An example of a basic Microgrid architecture is shown in Fig. 3.13, where two paralleled systems DG1 and DG2 are employed. Each DG system is comprised of a DC source, a pulse-width mod-

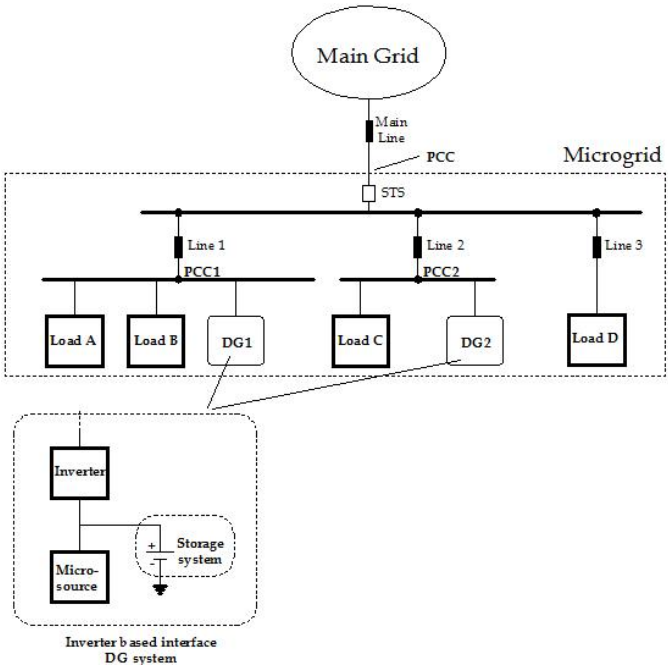

Fig. 3.13. Microgrid architecture diagram.

ulation VSI and LC filters. In this mode, the two DG systems are controlled to provide local power and voltage support for critical loads A, B and C. This configuration reduces the burden of generation and delivery of power directly from the main grid and enhances the immunity of critical loads to system disturbances in the grid ([43],[57].

As shown in Fig. 3.13, the Microgrid is connected to the main grid at its point of common coupling (PCC) usually through a static transfer switch (STS).

An important problem, that can be solved by the DG systems is the impact of unbalanced grid voltages (usually caused by unbalanced system faults or connected loads) on the overall system performance. If the unbalance in voltages is serious, STS opens to isolate the Microgrid from the main grid; however, also if the voltage unbalance is not so serious, STS may remain closed, resulting in sustained unbalanced voltages at PCC. Such a voltage unbalance can cause an increase in losses in motor loads (and hence motor overheating) and abnormal operation of sensitive equipments in the Microgrid.

Another issue regarding Microgrid is related to the ability of DG systems to increase system reliability and power quality due to the decentralization of supply. Indeed, using a decentralized control for each DG system, expensive communications systems can be avoided and problems connected to transient conditions in the grid (i.e. frequency oscillation) can be reduced.

3.8 Microgrid configuration

In the following will be presented the application of the combined *Voltage and Current control* strategy, in a simple distributed system in which several DG systems are contemporary connected to the same bus of a Microgrid. In particular, the Microgrid configuration under examination is shown in Fig. 3.14 and it consists in four DG systems, based on inverters connected to the main bus by different line impedances.

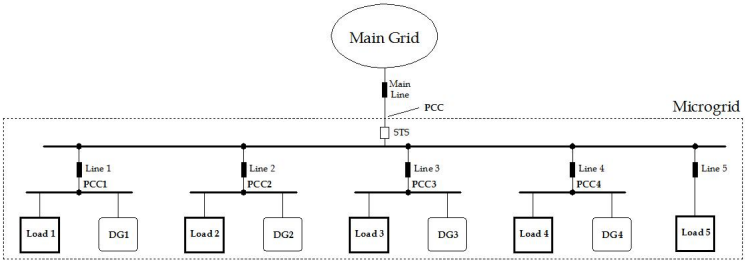

Fig. 3.14. Microgrid configuration considered.

Each DG is directly connected to a critical load that absorbs a different amount of active and reactive power for each phase. Besides, a linear and balanced load (Load 5) is connected at the main bus.

It is worth to underline that each DG system has merely information about the voltage at its own PCC and the currents absorbed from the critical load connected at the same PCC. Using this information, each DG system should operate in order to correct the power factor and to balance the active power absorbed by each phase of the load, so as to effect a regulation of the voltage and avoid that unbalances scatter in the main system. Obviously, each DG system provides active power to the grid supplying a share of the energy required by the loads in the Microgrid.

Thanks to the potentiality of the grid-connected inverters, the DG systems are able to influence the power flows of the Microgrid very quickly and in significant manner. However, a so fast action can bring out perturbations in the Microgrid and generate instability. Certainly, this can occur when many DG systems are present; for this reason, it is important that the DG systems control manages to avoid negative impacts on the Microgrid stability.

3.9 Power management

The choice of the desired instantaneous power flows P^* and Q^* has been effected in order to prove the benefits brought by the DG when many sources are present in a Microgrid. The value Q^* has been chosen equal to the reactive power absorbed by each local load in order to realize the load power factor correction and then to reduce the transmission losses. The desired active power flow P^* has been obtained as sum of two contributions. The former is equal for each phase to one third of the active power provided by the dc-power microsource. The other contribution is calculated in order to balance the power absorbed by an unbalanced load. In particular, the desired active power to be provided by each interfacing inverter on the $j-th$ phase has been chosen as

$$P_j^* = \Delta P_{LJ} + \frac{P_{ms}}{3}, \tag{3.28}$$

where P_{ms} is the instantaneous active power given by the microsource and ΔP_{LJ} is the difference between the power absorbed by the local load on the $j-th$ phase and the average power absorbed by all the phases, as shown by the following relationships:

$$\Delta P_{LJ} = P_{LJ} - P_{ave}, \quad P_{ave} = \frac{P_{La} + P_{Lb} + P_{Lc}}{3}, \tag{3.29}$$

3.10 Numerical results

Some numerical results have been carried out to demonstrate the effectiveness of the proposed application. The reactive power compensation obtained by the grid-connected inverters, controlled by the used control strategy for each PCC node and for a generic phase is displayed by Figg. 3.15, 3.16, 3.17, 3.18. They show as the reactive power absorbed by every local load is immediately compensated, when the control action for the instantaneous reactive power management starts at 0.1s; in fact each line current i_{Lh}

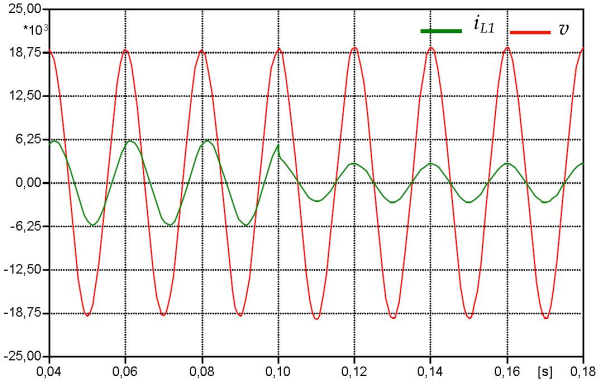

Fig. 3.15. Power factor correction for one phase of Load 1.

, with $h = 1, ..4$ (suitably amplified for necessity of visualization), is carried out in phase with each PCC voltage v and then it is also significantly reduced.

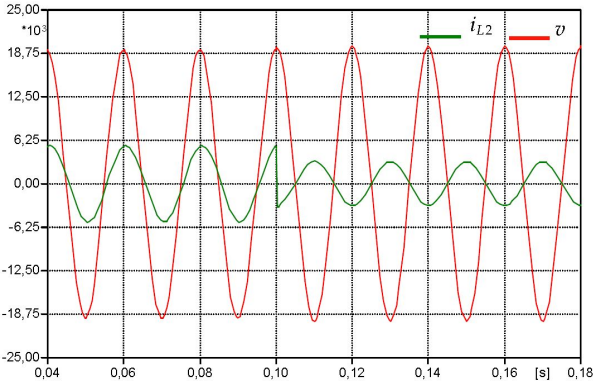

Fig. 3.16. Power factor correction for one phase of Load 2.

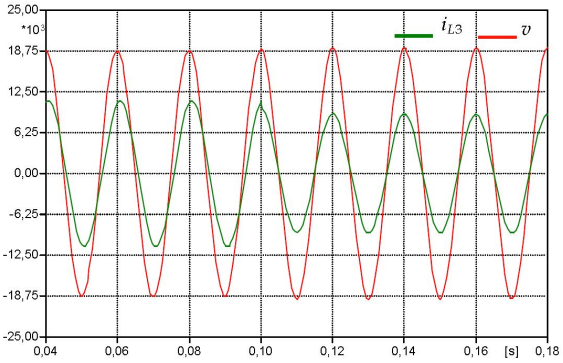

Fig. 3.17. Power factor correction for one phase of Load 3.

It is important to notice that the current i_{L2} is in opposition of phase with the voltage. This is because DG2 is able to produce more energy than that needed to its load and therefore the active power flow through Line 2 is inverted.

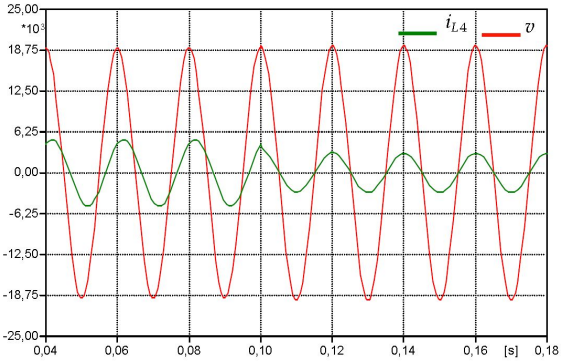

Fig. 3.18. Power factor correction for one phase of Load 4.

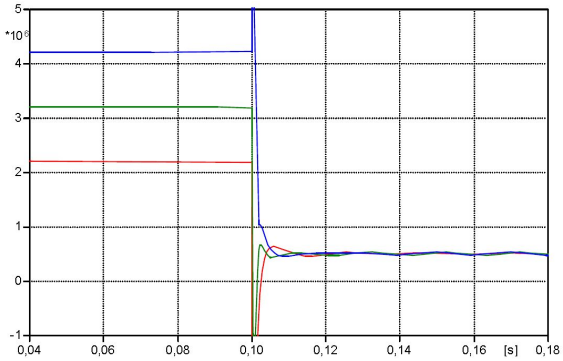

Fig. 3.19. Reduction of the instantaneous reactive powers provided by the main grid [Var].

Another effect of the reactive power compensation, carried out by all the DG systems, is clearly evidenced in Fig. 3.19. In fact, as a consequence of the reactive compensation the instantaneous reactive power supplied by the main grid for each phase is significantly reduced. This due to the fact that, in the operating conditions subsequently to the reactive compensation, the only load which needs reactive supply by the grid is the balanced Load 5, being far apart of the DG systems.

A further interesting result is presented in Fig. 3.20, that shows the effect of the power management used in order to balance the active power absorbed by the critical loads near the DG systems. As a consequence of the power management algorithm, each DG system, together with its critical load, is seen as a balanced Load from the main grid; in this way, the negative and zero current sequences present in the main grid currents are easily canceled before the compensation action, making so that the power provided by the main grid is balanced (see Fig. 3.21).

Finally, Fig. 3.22 points out that the power management made by the DG systems avoids that unbalanced currents can unbalance

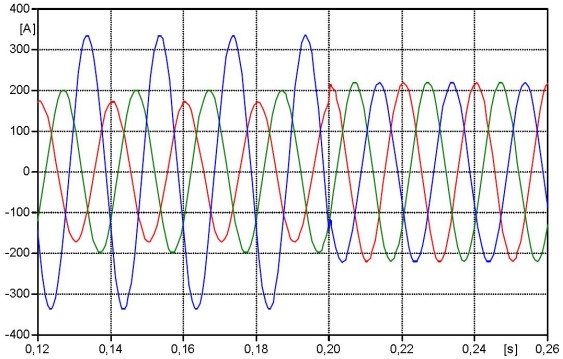

Fig. 3.20. Balancing of the main grid currents [A].

the main bus voltages. Therefore, also the balanced Load 5 absorbs the same value of instantaneous active power for each phase.

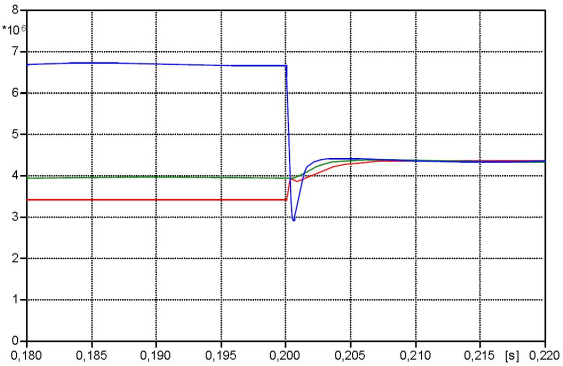

Fig. 3.21. Balancing of the main grid active powers [W].

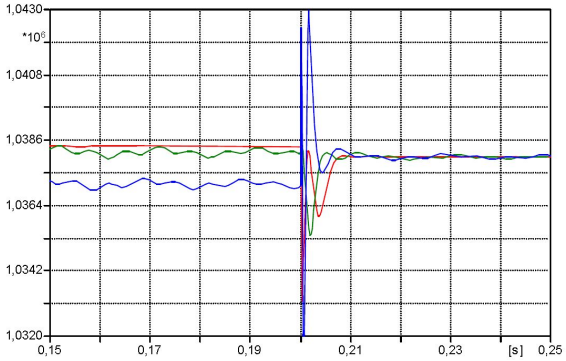

Fig. 3.22. Active powers absorbed by the Load 5 [W].

3.11 conclusion

In this chapter a control strategy for a PWM-VSI used as interface between a DC power source (photovoltaic cells, fuel cells, batteries and wind turbine generator with AC-DC converter) and the AC power distribution grid has been presented.

The proposed strategy is based on the combined action of a Voltage Control and a Current Control so as to utilize the advantages of both the control modes: accurate generation of the reference voltages and easy conditions on the stability of the whole system.

The paper has described in detail the outline of the proposed control strategy putting in evidence the synergetic action of the two control modes, for which the current control is constructed as support to the Voltage Control, without taking the place of it or even opposing it.

The numerical results confirm that the current control substantially acts only during a short transient and it finishes when the value of the current generated by the inverter has substantially reached the desired value; then, the support of the current

control part is practically equal to zero during the steady-state period.

Moreover, the chapter has dealt with the application of the control strategy presented in a Microgrid. First, this chapter has illustrated the concepts and control issues of Microgrids, which consist in clusters of loads and paralleled small DG systems operating as single power systems.

As clearly explained in the chapter, the microsources, used in the DG systems, having different output characteristics, in voltage and current, are connected to the utility grid using voltage source inverters based interfaces, usually known as grid-connected inverters. Due to the development of the power electronic devices, the grid-connected inverters are able to perform different useful functions such as the control of voltage and reactive power at the PCC of the generation source and a fast response to power quality events or fault conditions.

In particular, the control strategy has been applied to a Microgrid configuration, consisting in four DG systems, based on interfacing inverters connected to the main bus by different line impedances. Each DG is directly connected to a critical load that absorbs a different amount of active and reactive power for each phase. Besides, a linear and balanced load is connected at the main bus.

The application has been verified by various numerical simulations. In particular, the simulations have point out as, by using grid-connected inverter, the DG systems have been able to influence the power flows of the Microgrid very quickly and in significant manner. However, thanks to the good characteristics of the control strategy used, such fast performances have been achieved without generating perturbations and instability problems on the Microgrids. In fact, the numerical simulations show that the DG systems effectively provide services as reactive power compensation and load balancing without influence each other.

Conclusions

In this thesis we have focused on the study of control strategies, estimation methods and analysis techniques for distributed generation systems. In particular, the work faced the problem of integration of alternative energy resources with Electrical Power Systems, proposing innovative control architectures of power interfacing systems based on power converter.

The main topic were: the study of single-phase approach for frequency, amplitude, and phase estimation of grid voltages and current; the examination of modeling approach for electrical signals in power systems useful to develop new control strategies and analysis techniques for power electronic interfaces systems; and the develop of new power control strategies for grid-connected inverter.

To validate the results of the research carried out, for each topic, many laboratory and numerical experimental, which have been effected during the Ph.D course were presented.

List of pubblication

- D. Menniti, C. Picardi, A. Pinnarelli, D. Sgr, *Grid-connected inverters for alternative energy sources with a combined voltage and current control strategy*, International Conference on Clean Electrical Power, pp. 223-228, Capri (Italy), May 2007.
- C. Picardi, D. Sgr, *A new modelling approach for electrical signals for power systems*, International Symposium on Power Electronics, Electrical Drives, Automation and Motion (SPEEDAM 2008), pp. 912-917, Ischia (italy), Jun 2008.
- Menniti, D.; Picardi, C.; Pinnarelli, A.; Sgro, D.; *Power management by grid-connected inverters using a voltage and current control strategy for Microgrid applications*, International Symposium on Power Electronics, Electrical Drives, Automation and Motion (SPEEDAM 2008), pp. 1414 1419,Ischia (italy), 11-13 Jun. 2008.
- Coluccio, L.; Eisinberg, A.; Fedele, G.; Picardi, C.; Sgro, D.;*Modulating functions method plus SOGI scheme for signal tracking*, IEEE International Symposium on Industrial Electronics (ISIE 2008), pp. 854-859, Cambridge (United Kingdom), Jun. 30-Jul. 2 2008.
- Fedele, G.; Picardi, C.; Sgro, D.; *An estimation and synchronization method based on a new modeling approach of power*

electrical signals, International Conference on Renewable Energies and Power Quality (ICREPQ 2009), pp. 585-590, Valencia (Spain), 15-17 Apr. 2009.

- Picardi, C.; Sgro, D.;*Grid-connected inverter power flow control based on a new modeling approach of electrical signals* Clean Electrical Power, International Conference on Clean Electrical Power, pp. 585-590,Capri (Italy), Jun 2009.
- Fedele, G.; Picardi, C.; Sgro, D.; *A Power Electrical Signal Tracking Strategy Based on the Modulating Functions Method*, Transaction on IEEE Industrial Electronics, Vol. 56,No. 10, ISSN 0278-0046 , Oct. 2009, pp. 4079-4087.

Other publications:
Daniele Menniti, Ciro Picardi, Anna Pinnarelli and Domenico Sgro, *Application of a suitable control strategy for grid-connected inverters to the power management of a Microgrid*,Capitolo del libro:Distributed Generation, ISBN 978-953-7619-X-X. (Accepted by: IN-TECH, Vienna (Austria), in: 10/07/2009. final version sent in: 16/10/2009. Publication in: January 2009).

References

1. R. T. A. Timbus, M. Liserre and F. Blaabjerg. Synchronization methods for three phase distributed power generation systems. an overview and evaluation. Power Electronics Specialists Conference, June 2005.
2. R. D. H. T. M. S. B. Kroposki, C. Pink and P. Sen. Benefits of power electronic interfaces for distributed energy system. in Proc. Of Power Engineering Society General Meeting constant-frequency integration control, June 2006.
3. D. G. H. B. P. McGrath and J. J. H. Galloway. Power converter line synchronization using a discrete fourier transform (dft) based on a variable sample rate. *IEEE Trans. Power Electron.*, 20:877884, 2005.
4. L. S. Czarnecki. Instantaneous reactive power p-q theory and power properties of three-phase systems. *IEEE Trans. On Power Delivery*, 21:362–367, 2006.
5. A. T. de Almeida and P. S. Moura. *Energy Efficiency and Renewable Energy Handbook*, page 5.16. Taylor and Francis Group, 2007.
6. EREC. Integration of renewable energy sources, targets and benefits of large-scale deployment of renewable energy sources. Workshop on Renewable Energy Market Development Status and Prospects, April - May 2004.

7. M. L. F. Blaabjerg, R. Teodorescu and A. V. Timbus. Overview of control and grid synchronization for distributed power generation systems. *IEEE Trans. Ind. Electron.*, 53:13891409, 2006.
8. S. K. F. Blaabjerg, Z. Chen. Power electronics as efficient interface in dispersed power gebneration systems. *IEEE Trans. on Power Electronics*, 19:1184–1194, 2004.
9. A. A. F. De Mango, M. Liserre and A. Pigazo. Overview of anti-islanding algorithms for pv systems. part i: Axtive methods. in Proc. 12th International Power Electronics and Motion Control Conference, August-September 2006.
10. A. A. F. De Mango, M. Liserre and A. Pigazo. Overview of anti-islanding algorithms for pv systems. part i: Passive methods. in Proc. 12th International Power Electronics and Motion Control Conference, August-September 2006.
11. F. A. Farret and M. G. Simões. *Integration of Alternative Source of Energy.* IEEE Press, 2006.
12. V. Friedman. A zero crossing algorithm for the estimation of the frequency of a single sinusoid in white noise. *IEEE Trans. Signal Process.*, 42:15651569, 1994.
13. D. H. R. B. W. D. G. Pepermans, J. Driesen. Distributed generation: definition, benefits and issues. *Energy Policy*, 33:787–798, 2005.
14. D. Y. Goswami and F. Kreith. *Energy Efficiency and Renewable Energy Handbook*, pages 1.1–1.2. Taylor and Francis Group, 2007.
15. A. N. H. Akagi, Y. Kanagawa. Instantaneous reactive power compensator comprising switching devices without energy storage components. *IEEE Trans. On Industry Application*, 20:625–630, 1984.
16. M. A. H. Akagi, E. H. Watanabe. *Instantaneous power theory and applications to power conditioning.* IEEE Press, 2007.
17. T. Hayward. Bp statistical review of world energy, 2009. Technical report, British Petroleum Corporation, British Petroleum, London, 2009.
18. G. C. Hsieh and J. C. Hung. Phase-locked loop techniques. a survey. *IEEE Trans. Ind. Electron.*, 43:609615, 1996.
19. J. R. E. J. R. Rodriguez, J. W. Dixon and J. Pontt. Pwm regenerative rectifiers: State of the art. *IEEE Trans. on Industrial Electronics*, 52:5–22, 2005.
20. H. S.-R. J. R. Trapero and V. F. Batlle. An algebraic frequency estimator for a biased and noisy sinusoidal signal. *Signal Processing*, 87:1188–1201, 2007.

21. D. Jovcic. Phase locked loop system for facts. *IEEE Trans. Power Syst.*, 18:11161124, 2003.
22. S. A. Kalogirou. *Solar Energy Engineering: Processes and Systems*. Academic Press, 2009.
23. M. Karimi-Ghartemani and M. R. Irvani. A new phase-locked loop (pll) system. in Proc. IEEE Midwest Symp. Circuits Syst., August 2001.
24. M. Karimi-Ghartemani and H. Karimi. Processing of symmetrical components in time-domain. *IEEE Trans. Power Syst.*, 22:572579, 2007.
25. V. Kaura and V. Blasko. Operation of a phase locked loop system under distorted utility condition. *IEEE Trans. Ind. Appl.*, 33:58–63, 1997.
26. G. F. C. P. L. Coluccio, A. Eisinberg and D. Sgró. Modulating functions method plus sogi scheme for signal tracking. in Proc. IEEE International Symposium on Industrial Electronics, June-July 2008.
27. A. Landi and L. Sani. Modulating functions for modelling pwm switching converters. in Proc. Inst. Elect. Eng.Electr. Power Appl., July 2005.
28. R. H. Lasseter. Microgrids. Technical report, Institute of Electrical and Elctronics Engineers, 2002.
29. S. S. L.N. Arruda and B. C. Filho. Pll structures for utility connected systems. in Proc. Industry Applications Conference, September-October 2001.
30. P. locked loop for grid-connected three-phase power conversion systems. A new phase-locked loop (pll) system. in Proc. Inst. Elect. Eng.Electr. Power Appl., May 2000.
31. J. M. M. Aredes L. F. C. Monteiro. Control strategies for series and shunt active filters. in Proc. Of Power Techn. Conference, June 2003.
32. R. T. M. Ciobotaru and V. Agelidis. Offset rejection for pll based synchronization in grid-connected converters. in Proc. IEEE Applied Power Electronics Conference and Exposition, February 2008.
33. R. T. M. Ciobotaru and F. Blaabjerg. Improved pll structures for single-phase grid inverters. in Proc. POWER ELECTRONICS AND INTELLIGENT CONTROL FOR ENERGY CONSERVATION, October 2005.
34. R. T. M. Ciobotaru and F. Blaabjerg. A new single-phase pll structure based on second order generalized integrator. in Proc.

POWER ELECTRONICS AND INTELLIGENT CONTROL FOR ENERGY CONSERVATION, June 2006.
35. V. A. M. Ciobotaru and R. Teodorescu. Accurate and less-disturbing active anti-islanding method based on pll for grid-connected pv inverters. in Proc. Power Electronics Specialists Conference, June 2008.
36. H. K. M. Karimi-Ghartemani and M. R. Irvani. A magnitude/phase-locked loop system based on estimation of frequency and inphase/quadrature-phase amplitudes. *IEEE Trans. Ind. Electron.*, 51:511517, 2004.
37. A. D. M. Liserre, A. Pigazo and V. Moreno. An anti-islanding method for single-phase inverters based on a grid voltage sensorless control. *IEEE Trans. Ind. Electron.*, 53:1418–1426, 2006.
38. S. D. M. M. Begović, P. M. Djuric and A. G. Phadke. Frequency tracking in power networks in the presence of harmonics. *IEEE Trans. Power Del.*, 8:480486, 1993.
39. C. J. M. Mboup and M. Fliess. A revised look at numerical differentiation with an application to nonlinear feedback control. in Proc. Of the 15th Mediterranean Conference on Control and Automation, July 2007.
40. E. A. D. of International Energy Agency. World energy outlook, 2004. Technical Report ISBN: 92-64-10949-8, International Energy Agency, France, Paris, October 2005.
41. E. A. D. of International Energy Agency. World energy outlook, 2005. Technical Report ISBN: 92-64-10949-8, International Energy Agency, France, Paris, October 2005.
42. L. B. of Madingley. Bp statistical review of world energy, 2006. Technical report, British Petroleum Corporation, British Petroleum, London, 2006.
43. G. V. P. Flannery and B. Shi. Integration of distributed technologies standard power electronic interfaces. Technical report, California Energy Commission Consultant Report, 2004.
44. E. H. W. P. G. Barbosa, L. B. G. Rolim and R. Hanitsch. Control strategy for grid-connected dc-ac converters with load power factor correction. in IEE Proc. Of Generation, Transmission and Distribution, September 1998.
45. J. B. J. C. R. B. P. Rodriguez, J. Pou and D. Boroyevich. Decoupled double synchronous reference frame pll for power converters control. *IEEE Trans. Power Electr.*, 22:584–592, 2007.

46. A. G.-C. P.Garcìa-Gonzàlez. Control system for a pwm-based statcom. *IEEE Trans. On Power Delivery*, 15:1252–1257, 2000.
47. H. A. Preisig and D. W. T. Rippin. Theory and application of the modulating function methodi. review and theory of the method and theory of the spline-type modulating functions. *Comput. Chem. Eng.*, 17:1–16, 1993.
48. C. Qiao and K. M. Smedley. Three-phase grid-connected inverters interface for alternative energy sources with unified constant-frequency integration control. in Proc. Of IAS 2001 Conference, September 2001.
49. V. Quaschning. *Understanding Renewable Energy Systems*. EARTHSCAN, 2005.
50. F. P. D. R. Weidenbrüg and R. Bonert. New synchronization method for thyristor power converters to weak ac-systems. *IEEE Trans. Ind. Electron.*, 40:505511, 1993.
51. S. E. A. M. D. S. Rezk, C. Join and M. Bedoui. Frequency change-point detection in physiological signals: an algebraic approach. *Int. Journal on Science and Techniques of Automatic control and computer engineering*, 2:1–13, 2008.
52. S. Sahah and V. Sundarsingh. Novel grid-connected photovoltaic inverter. in IEEE Proc. Of Gener. Transm. Distrib., March 1996.
53. R. N. S.A.O. da Silva, E. Tomizaki and E. Coelho. Pll structures for utility connected systems under distorted utility conditions. in Proc. 32nd Annual Conference IEEE Industrial Electronics, IECON, November 2006.
54. B. F. R. C. S.M. Silva, B.M. Lopes and W. Bosventura. Performance evaluation of pll algorithms for single-phase grid-connected systems. in Proc. IAS Annual Meeting Industry Applications Conference, October 2004.
55. A. P. V. M. Moreno, M. Liserre and A. DellAquila. A comparative analysis of real-time algorithms for power signal decomposition in multiple synchronous reference frames. *IEEE Trans. Power Electron.*, 22:12801289, 2007.
56. O. Vainio and S. J. Ovaska. Noise reduction in zero crossing detection by predictive digital filtering. *IEEE Trans. Ind. Electron.*, 42:5862, 1995.
57. P. L. Y. W. Li, D. M. Vilathgamuwa. Design, analysis, and real-time testing of a controller for multibus microgrid system. *IEEE Trans. On Power Electronics*, 19:1195–1204, 2004.